



THE HONG KONG
POLYTECHNIC UNIVERSITY

香港理工大學

Pao Yue-kong Library

包玉剛圖書館

Copyright Undertaking

This thesis is protected by copyright, with all rights reserved.

By reading and using the thesis, the reader understands and agrees to the following terms:

1. The reader will abide by the rules and legal ordinances governing copyright regarding the use of the thesis.
2. The reader will use the thesis for the purpose of research or private study only and not for distribution or further reproduction or any other purpose.
3. The reader agrees to indemnify and hold the University harmless from and against any loss, damage, cost, liability or expenses arising from copyright infringement or unauthorized usage.

IMPORTANT

If you have reasons to believe that any materials in this thesis are deemed not suitable to be distributed in this form, or a copyright owner having difficulty with the material being included in our database, please contact lbsys@polyu.edu.hk providing details. The Library will look into your claim and consider taking remedial action upon receipt of the written requests.



The Hong Kong Polytechnic University
Department of Civil and Environmental Engineering

**BEHAVIOR OF FRP-CONFINED SELF-
COMPACTING CONCRETE**

FANG Xiaoliang

**A Thesis Submitted in Partial Fulfillment of the Requirements for
the Degree of Master of Philosophy**

February 2014

To My Parents

CERTIFICATE OF ORIGINALITY

I hereby declare that this thesis is my own work and that, to the best of my knowledge and belief, it reproduces no material previously published or written, nor material that has been accepted for the award of any other degree or diploma, except for where due acknowledgement has been made in the text.

(Signed)

Xiaoliang FANG (Name of student)

ABSTRACT

With the advantages of excellent corrosion resistance and high strength-to-weight ratios, FRP composites are being increasingly used in both structural retrofit/strengthening and new construction. In the new construction area, hybrid FRP-concrete members based on filament-wound FRP confining tubes with fibers oriented close to the hoop direction have great potential in practical applications. Such members include concrete-filled FRP tubes with longitudinal internal steel reinforcement and FRP-steel-concrete double-skin tubular columns (DSTCs).

This thesis is concerned with the behavior of self-compacting concrete (SCC) used to fill FRP confining tubes to form hybrid members of various forms. In such hybrid members, the use of SCC is highly attractive as it simplifies the task of construction and facilitates the proper flow of concrete into small spaces (e.g. the annular space in a DSTC). While the substitutability of SCC for normal concrete (NC) is widely accepted based on numerous studies, little knowledge exists on the differences between SCC and NC when they are under substantial confinement from an FRP tube. As extensive work has been published on FRP-confined NC, this thesis presents a systematic study on the behavior of FRP-confined SCC as found in concrete-filled FRP confining tubes, and compares this behavior with that of FRP-confined NC.

Following a literature review that identifies the existing knowledge gaps, this thesis presents an experimental study on the behavior of SCC confined by an FRP wrap under axial compression. The FRP wrap had fibers oriented only in the hoop direction and was formed on the concrete column after the concrete had hardened. As a result, these tests did not involve a number of complicating effects associated with concrete-filled FRP tubes, including the complexity in determining the hoop elastic modulus, the effect of the axial stiffness of the FRP tube and the shrinkage of the SCC. The test results are carefully presented and compared with an accurate stress-strain model for FRP-confined NC (i.e. Jiang and Teng's model). The comparisons indicate that the model can provide reasonably close predictions for the axial stress-axial strain behavior of moderately-confined and heavily-confined normal strength SCC and heavily-confined high strength SCC but fails to make close predictions for the axial stress-axial strain behavior of weakly-confined SCC and moderately-confined high strength SCC. In addition, the model does not provide accurate predictions for the lateral expansion of FRP-confined SCC.

The thesis next presents a study on the behavior of SCC in glass FRP (GFRP) tubes by testing a series of SCC-filled GFRP tubes under axial compression. An expansive admixture was included in the SCC mix for some of the specimens to compensate for the shrinkage of SCC. The test results of SCC-filled GFRP tubes indicate that a suitable amount of expansive admixture should be used in such columns to create a better confinement condition. The test results are again compared with predictions from Jiang

and Teng's model developed for FRP-confined NC. These comparisons again show that the lateral expansion behavior of SCC confined by GFRP tubes cannot be properly predicted by the model, which however can predict the axial stress-axial strain behavior of SCC confined by GFRP tubes reasonably closely, particularly when the shrinkage of SCC is compensated for through the use of an expansive admixture.

ACKNOWLEDGMENTS

First of all, and most importantly, I would like to express my sincere gratitude to my supervisor, Professor Jin-Guang Teng, for providing me with a precious chance of being his student and the opportunity of doing research, and for illuminating me with the valuable qualities of being an excellent researcher. During the period of my MPhil study, Professor Teng has provided me with patient and meticulous help that will benefit me in the rest of my life.

Secondly, but equally importantly, I would like to express my love from the bottom of my heart to my parents who have nurtured me and supported me throughout my whole life no matter what I have done or have faced. And they are the persons to whom this thesis is dedicated.

I also wish to give my heartfelt thanks to my co-supervisor, Dr. Tao Yu, without whom I would not have been able to finish my MPhil study. And the same thanks also go to Dr. Lik Lam, who helped me with the design and understanding of the properties of self-compacting concrete.

I would like to give my special thanks to those people who helped me during my MPhil

study: the other members of our research group, including but not limited to Mr. Bing Zhang, Dr. Qiong-Guan Xiao, Mr. Guan Lin, Mr. Yi-Nan Yang, and Mr. Bing Fu; and my friends, including Mr. Xiao Liu, Miss Yi-Xin Peng, Mr. Bao-Jian Zhan, Mr. Bo Li and Miss Bin-Yu Zhang, who not only helped me with my research work but also brought happiness to my life and made it unforgettably wonderful.

The same thanks also go to all the technicians who helped me with my experimental work.

Finally, I wish to thank The Hong Kong Polytechnic University for offering me a good research environment and rich research resources.

CONTENTS

CERTIFICATE OF ORIGINALITY	III
ABSTRACT	IV
ACKNOWLEDGMENTS	VII
LIST OF TABLES.....	XIII
LIST OF FIGURES	XIV
CHAPTER 1 INTRODUCTION.....	1
1.1 GENERAL	1
1.2 RESEARCH OBJECTIVES AND SIGNIFICANCE	3
1.2.1 Research objectives.....	3
1.2.2 Research significance.....	3
1.3 RESEARCH METHODOLOGY	4
1.4 OUTLINE OF THE THESIS	5
1.5 FIGURES	7
1.6 REFERENCES.....	8
CHAPTER 2 LITERATURE REVIEW	10
2.1 INTRODUCTION	10
2.2 UNCONFINED SELF-COMPACTING CONCRETE (SCC).....	10

2.2.1	Properties of SCC.....	11
2.2.2	Effects of mix proportions of SCC.....	12
2.2.3	Confined SCC	14
2.3	STRESS-STRAIN MODELS FOR FRP-CONFINED NORMAL CONCRETE.....	15
2.3.1	General	15
2.3.2	Analysis-oriented models.....	15
2.4	PREDICTION OF THE MATERIAL PROPERTIES OF GFRP TUBES	18
2.5	TESTING STANDARDS FOR FRP TUBES	18
2.5.1	Tensile coupon tests	19
2.5.2	Split-disk tests	20
2.5.3	Axial compression tests	21
2.6	CONCLUSIONS.....	22
2.7	FIGURES	24
2.8	REFERENCES.....	26
CHAPTER 3 AXIAL COMPRESSIVE BEHAVIOR OF SCC CONFINED BY AN FRP WRAP		29
3.1	INTRODUCTION	29
3.2	EXPERIMENTAL PROGRAM.....	29
3.2.1	Test specimens	29
3.2.2	Mix design.....	31

3.2.3	Test set-up and instrumentation	33
3.3	TEST RESULTS AND DISCUSSIONS	34
3.3.1	Test results.....	34
3.3.2	General behavior	35
3.3.3	Axial stress-strain behavior.....	35
3.3.4	Axial strain-hoop strain relationship.....	37
3.3.5	Hoop rupture strains.....	38
3.4	COMPARISON WITH JIANG AND TENG'S (2007) MODEL	39
3.5	CONCLUSIONS.....	43
3.6	FIGURES	45
3.7	REFERENCES.....	52
CHAPTER 4 AXIAL COMPRESSIVE BEHAVIOR OF SCC-FILLED GFRP TUBES		56
4.1	INTRODUCTION	56
4.2	EXPERIMENTAL PROGRAM.....	57
4.2.1	Test specimens	57
4.2.2	Mix design and properties of SCC.....	58
4.2.3	Properties of GFRP tubes.....	59
4.2.4	Test set-up and instrumentation	63
4.3	TEST RESULTS AND DISCUSSIONS	63
4.3.1	Expansion of SCC.....	63
4.3.2	General behavior	64

4.3.3	Axial load-strain relationship.....	64
4.3.4	Axial stress-strain behavior.....	66
4.3.5	Axial strain-hoop strain relationship.....	70
4.4	HOOP RUPTURE STRAINS	70
4.5	CONCLUSIONS.....	71
4.6	FIGURES	72
4.7	REFERENCES.....	95
CHAPTER 5	CONCLUSIONS	96
5.1	INTRODUCTION	96
5.2	COMPRESSIVE BEHAVIOR OF SCC CONFINED BY FRP WRAPS	96
5.3	COMPRESSIVE BEHAVIOR OF SCC CONFINED BY GFRP TUBES	98
5.4	FUTURE RESEARCH	99

LIST OF TABLES

Table 3.1 Details of test specimens	31
Table 3.2 Mix design of SCC	33
Table 3.3 Key test results	34
Table 4.1 Details of test specimens	58
Table 4.2 Mix design for SCC-filled GFRP tubes	59
Table 4.3 Key test results of SCC-filled FRP tubes	67

LIST OF FIGURES

Figure 1.1 Hybrid FRP-concrete tubular columns	7
Figure 2.1 Typical test fixture of split-disk tests (Reproduced from ASTM D2290)	24
Figure 2.2 Typical split-disk test specimens (Reproduced from ASTM D2290)....	24
Figure 2.3 End-strengthened test specimens (Reproduced from GB 5350).....	25
Figure 3.1 Layout of strain gauges.....	45
Figure 3.2 Test set-up	45
Figure 3.3 Typical failure mode of CFRP and GFRP jacket.....	46
Figure 3.4 Axial stress-strain curves	47
Figure 3.5 Axial strain-hoop strain curves	49
Figure 3.6 Hoop rupture strain distribution around the circumference.....	50
Figure 3.7 Comparison with Jiang and Teng's (2007) model.....	51
Figure 4.1 Hoop and axial stress-strain curves from split-disk tests for D200 specimens	72
Figure 4.2 Hoop and axial stress-strain curves from split-disk tests for D300 specimens	72
Figure 4.3 Hoop stress-strain curves from split-disk tests of specimens with fiber angles of ± 80 degrees with the diameters of 200mm and 300mm.....	73

Figure 4.4 Failure mode of split-disk test specimens (D200 specimens)	74
Figure 4.5 Failure mode of split-disk test specimens (D300 specimens)	74
Figure 4.6 Axial stress-strain curves of the D200 specimens tested by Mr. Zhang Bing	75
Figure 4.7 Failure mode of ring specimens under axial compression	76
Figure 4.8 Layout of eight groups of strain gauges	77
Figure 4.9 Pre-test monitoring results of specimens 84-0-I & 84-0-II	77
Figure 4.10 Pre-test monitoring results of specimens 84-8-I & 84-8-II	78
Figure 4.11 Pre-test monitoring results of specimens 84-12-I & 84-12-II.....	79
Figure 4.12 Pre-test monitoring and concrete curing.....	80
Figure 4.13 Failure mode of specimens 84-0-I & 84-0-II.....	81
Figure 4.14 Failure mode of specimens 84-8-I & 84-8-II.....	81
Figure 4.15 Failure mode of specimens 84-12-I & 84-12-II.....	82
Figure 4.16 Comparison between axial strain gauge values and LVDT readings ..	83
Figure 4.17 Load-displacement curves of specimens	85
Figure 4.18 Stress-strain curves of SCC-filled GFRP tubes	86
Figure 4.19 Stress-strain curves excluding the GFRP tube axial contribution	88
Figure 4.20 Stress-strain curves with and without GFRP tube axial contribution of the 6 specimens	91
Figure 4.21 Axial-to-hoop strain curves of SCC-filled GFRP tubes.....	92
Figure 4.22 Hoop rupture strain distribution around the circumference of specimens	94

CHAPTER 1

INTRODUCTION

1.1 GENERAL

The hybrid use of fiber reinforced polymer (FRP) composites with traditional structural materials (e.g. steel and concrete) to create hybrid structures has received much research attention worldwide (Mirmiran 2003; Cheng and Karbhari 2006; Teng et al. 2007). Because of their excellent corrosion resistance, hybrid FRP-concrete tubular columns have great potential for use as compression members in outdoor structures (e.g. bridges and coastal structures) which are likely to be exposed to a harsh environment. Two typical examples of hybrid FRP-concrete tubular columns are concrete-filled FRP tubes (CFFTs) which consist of an outer FRP tube filled with plain or steel-reinforced concrete (Mirmiran and Shahawy 1997; Fam and Rizkalla 2001), and hybrid FRP-concrete-steel double-skin tubular columns (DSTCs) which consist of an outer FRP tube, an inner steel tube and an annular concrete infill in between (Teng et al. 2007; Yu et al. 2010) (see Figure 1.1).

In the construction of hybrid FRP-concrete tubular columns, the use of self-compacting concrete (SCC) is attractive. Indeed, SCC has become increasingly popular in recent years, particularly in constructing heavily-reinforced concrete structures and those cast with a

stay-in-place form where the quality of concrete is difficult to control and/or examine (Bonen & Shah 2005; Paultre et al. 2005). The use of SCC is particularly attractive in constructing hybrid DSTCs where the concrete layer is relatively thin. In hybrid FRP-concrete tubular columns, the concrete is subjected to confinement from the FRP tube (and from the inner steel tube in the case of hybrid DSTCs), and its behavior is quite different from unconfined concrete. While many studies have been conducted on confined normal concrete (NC) (e.g. Lam and Teng 2003; Jiang and Teng 2007), research on confined SCC (e.g. steel-confined SCC and FRP-confined SCC) has been very limited (Han & Yao 2004; El-Chabib et al. 2005; Han et al. 2005; Lachemi et al. 2006). The few existing studies have shown that the behavior of confined SCC is generally similar to that of confined NC, but differences between the two were also noted by some researchers (e.g. El-Chabib et al. 2005; Lachemi et al. 2006). Lachemi et al. (2006) tested several series of concrete-filled steel tubular columns with either NC or SCC and concluded that the confined strength of SCC is considerably lower than that of NC. El-Chabib et al. (2005) presented the only available existing study on FRP-confined SCC where a total of 12 short CFFTs with SCC were tested under axial compression. In El-Chabib et al.'s (2005) tests, a single type of FRP tube was used, and the SCC had similar unconfined strengths (i.e. around 37 MPa); the FRP tubes used all had fibers oriented at $\pm 55^\circ$ with respect to the longitudinal axis and thus had a substantial axial stiffness. El-Chabib et al. (2005) noted from their test results that the stress-strain curves of FRP-confined SCC were different from those of FRP-confined NC in the transition region of the curve (i.e. the

region connecting the first portion which is similar to that of unconfined concrete and the second portion when the FRP has been effectively activated).

Against this background, this thesis presents an in-depth study to gain a better understanding of the behavior of FRP-confined SCC, and to clarify any differences between FRP-confined NC and SCC.

1.2 RESEARCH OBJECTIVES AND SIGNIFICANCE

1.2.1 Research objectives

The specific objectives of the MPhil study are to:

- 1) Obtain a good understanding of SCC confined by an FRP wrap through a series of axial compression tests;
- 2) Obtain a good understanding of confined SCC in FRP tubular columns through a series of axial compression tests;
- 3) Compare the behavior of FRP-confined SCC with that of FRP-confined NC by making use of an existing stress-strain model for the latter; and
- 4) Clarify the effect of expansive admixture on the behavior of FRP-confined SCC.

1.2.2 Research significance

Hybrid FRP-concrete tubular columns possess a number of important advantages over existing forms of columns, including their excellent corrosion resistance. Corrosion of

steel reinforcement has been the main cause of the massive infrastructure deterioration problem faced by countries/regions around the world, including Hong Kong and the rest of China. Hybrid FRP-concrete tubular columns therefore have special relevance to Hong Kong and the rest of China due to their enormous construction activities. The use of self-compacting concrete will facilitate the construction (and possibly improve the construction quality) of hybrid FRP-concrete tubular columns.

1.3 RESEARCH METHODOLOGY

The MPhil research program included the following three parts:

- 1) A series of axial compression tests was conducted on SCC confined by an FRP wrap.

The test parameters included the unconfined concrete strength and the thickness and type of the FRP wrap;
- 2) A series of axial compression tests was conducted on hybrid FRP-concrete tubular columns filled with SCC, where filament-wound FRP tubes were used. The test parameters included the amount of expansive admixture to examine that effect.
- 3) Theoretical analysis was conducted by making use of Jiang and Teng's (2007) analysis-oriented stress-strain model. The predictions from Jiang and Teng's (2007) model were compared with the experimental results obtained in the present study.

1.4 OUTLINE OF THE THESIS

This thesis consists of five chapters, details of which are summarized below.

Chapter 2 presents a literature review of topics related to the present study. The review includes existing studies on self-compacting concrete, stress-strain models for confined concrete, and relevant material testing standards.

Chapter 3 first presents a series of axial compression tests on SCC confined by an FRP wrap. A brief introduction to the test program is first given, followed by the experimental observations, results and discussions. Predictions from Jiang and Teng's (2007) stress-strain model are then compared with the experimental results, clarifying the difference between FRP-confined SCC and FRP-confined NC.

Chapter 4 first presents a series of axial compression tests on SCC filled FRP tubes, including associated material tests for the filament-wound FRP tubes. The specimen details, material properties, preparation of specimens, test set-up and instrumentation are described in detail. The experimental results are next presented and discussed, to clarify the effect of expansive admixture on confinement effectiveness. Comparisons between the test results and predictions from Jiang and Teng's (2007) model are also presented.

The thesis closes with Chapter 5, where the conclusions drawn from previous chapters

are reviewed, and areas in need of further research highlighted.

1.5 FIGURES

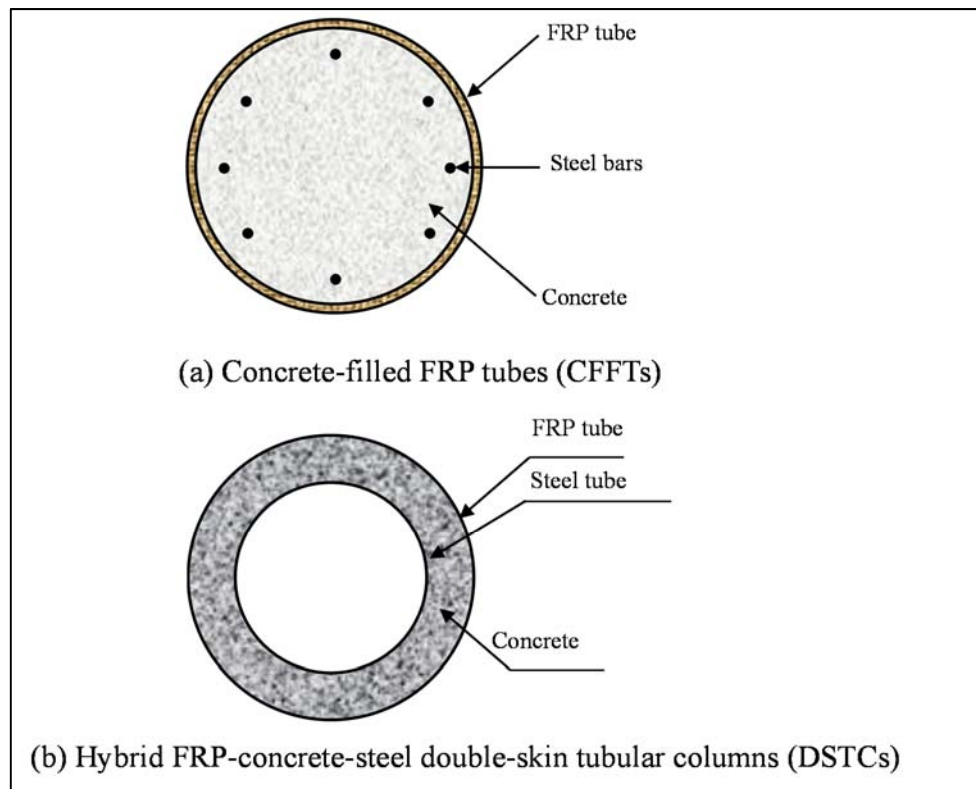


Figure 1.1 Hybrid FRP-concrete tubular columns

1.6 REFERENCES

- BONEN, D. & SHAH, S. P. 2005. Fresh and hardened properties of self - consolidating concrete. *Progress in Structural Engineering and Materials*, Vol. 7, No. 1, pp. 14-26.
- CHENG, L. & KARBHARI, V. M. 2006. New bridge systems using FRP composites and concrete: a state - of - the - art review. *Progress in Structural Engineering and Materials*, Vol. 8, No. 4, pp. 143-154.
- EL CHABIB, H., NEHDI, M. & EL NAGGAR, M. H. 2005. Behavior of SCC confined in short GFRP tubes. *Cement and Concrete Composites*, Vol. 27, No. 1, pp. 55-64.
- FAM, A. Z. & RIZKALLA, S. H. 2001. Confinement model for axially loaded concrete confined by circular fiber-reinforced polymer tubes. *ACI Structural Journal*, Vol. 98, No. 4, pp. 451-461.
- HAN, L. H. & YAO, G. H. 2004. Experimental behaviour of thin-walled hollow structural steel (HSS) columns filled with self-consolidating concrete (SCC). *Thin-walled Structures*, Vol. 42, No. 9, pp. 1357-1377.
- HAN, L. H., YAO, G. H. & ZHAO, X. L. 2005. Tests and calculations for hollow structural steel (HSS) stub columns filled with self-consolidating concrete (SCC). *Journal of Constructional Steel Research*, Vol. 61, No. 9, pp. 1241-1269.
- JIANG, T. & TENG, J. G. 2007. Analysis-oriented stress-strain models for FRP-confined concrete. *Engineering Structures*, Vol. 29, No. 11, pp. 2968-2986.
- LACHEMI, M., HOSSAIN, K. M. A. & LAMBROS, V. B. 2006. Axial load behavior of

self-consolidating concrete-filled steel tube columns in construction and service stages. *ACI Structural Journal*, Vol. 103, No. 1, pp. 38-47.

LAM, L. & TENG, J. G. 2003. Design-oriented stress-strain model for FRP-confined concrete. *Construction and Building Materials*, Vol. 17, No. 6-7, pp. 471-489.

MIRMIRAN, A. 2003. Stay-in-place FRP form for concrete columns. *Advances in Structural Engineering*, Vol. 6, No. 3, pp. 231-241.

MIRMIRAN, A. & SHAHAWY, M. 1997. Behavior of concrete columns confined by fiber composites. *Journal of Structural Engineering*, Vol. 123, No. 5, pp. 583-590.

PAULTRE, P., KHAYAT, K. H., CUSSON, D. & TREMBLAY, S. 2005. Structural performance of self-consolidating concrete used in confined concrete columns. *ACI Structural Journal*, Vol. 102, No. 4, pp. 560-568.

TENG, J. G, HUANG, Y. L, LAM, L. & YE, L. 2007. Theoretical model for fiber-reinforced polymer-confined concrete. *Journal of Composites for Construction*, Vol. 11, No. 2, pp. 201-210.

YU, T., TENG, J. G. & WONG, Y. L. 2010. Stress-strain behavior of concrete in hybrid FRP-concrete-steel double-skin tubular columns. *Journal of Structural Engineering*, Vol. 136, No. 4, pp. 379-389.

CHAPTER 2

LITERATURE REVIEW

2.1 INTRODUCTION

This chapter presents a review of existing studies on the topics related to the present study. The review includes the following topics: (1) self-compacting concrete (SCC), with a particular focus on the comparison of its properties with those of normal concrete (NC); (2) existing stress-strain models for FRP-confined concrete which were proposed based on studies on normal concrete; and (3) relevant material testing standards for filament-wound FRP tubes.

2.2 UNCONFINED SELF-COMPACTING CONCRETE (SCC)

Self-compacting concrete has become more and more attractive since its invention in Japan in the mid-1980s, especially in concrete structures which are heavily-reinforced and tubular columns. Extensive research has been conducted on SCC (Bonen and Shah, 2005, Domone, 2007, Mazzotti et al., 2006). Existing studies on unconfined SCC have been focused on the following issues: 1) the properties of SCC; 2) the effects of mix proportion (e.g. the use of admixture) on its behavior; and 3) the bond between SCC and other materials. The review presented below is focused on the first two issues which are

directly related to the present study.

2.2.1 Properties of SCC

Normal concrete has been applied in construction for a long time and the main properties of normal concrete are now well understood. Research on the properties of SCC normally relies on those of NC as a reference. Among the existing publications, Domone (2007) presents a review of existing studies, which is very useful for a basic understanding of the properties of SCC. It was concluded by Domone (2007) that the properties of SCC are generally similar to those of NC although some differences do exist: (1) the ratio of cylinder compressive strength to cube compressive strength of SCC varies from about 0.8 to near 1 and is generally greater than that of NC except when the concrete strength is low (e.g. cube compressive strength = 30MPa); (2) the ratio of tensile strength to compressive strength of SCC is similar to that of NC; (3) the elastic modulus of SCC can be up to 40% lower than that of NC when the compressive strength is low (e.g. cube compressive strength = 20 MPa), but the difference reduces to less than 5% when the compressive strength is high (e.g. cube compressive strength = 90–100 MPa); (4) existing studies showed conflicting results on certain properties (e.g. toughness and ductility) of SCC which needed more research work. Domone (2007) also concluded that the variation of in-situ properties of SCC in structural members is similar to that of NC; the mix design of SCC is the key factor dictating its performance but for NC site practice has the greatest influence.

Besides the studies summarized in Domone (2007), there are also other studies which focused on specific aspects of SCC. Panesar and Shindman (2011) provided a new measurement method, namely, the ultrasonic pulse velocity (UPV) measurements, in order to analyze the elastic properties of SCC. This method, together with dynamic-to-static elastic modulus ratios at different ages obtained from experiments, can be used to determine the compressive strength of SCC. Mazzotti et al. (2006) investigated the creep and shrinkage of SCC. Considering the evolution of strength and elastic modulus with the development of shrinkage and creep deformations, a simplified non-linear model was proposed by these researchers to predict the creep and shrinkage of SCC based on extensive test results. Many studies have also been conducted on the behavior of SCC from a microstructure perspective. Most of these studies were focused on the effects of a particular chemical compound. Among these studies, Tragardh (1999) found that SCC has a denser microstructure than NC for the same water/cement ratio, which is one of the key factors responsible for the differences in properties between SCC and NC.

2.2.2 Effects of mix proportions of SCC

Similar to NC, the properties of SCC depend much on the constituent materials and mix proportions. This has attracted extensive research attention.

A number of studies (e.g. Detwiler and Mehta 1989; Kwan 2000) have been concerned with the use of adding silica fume in SCC. These studies suggested that the addition of

silica fume increases not only the strength but also the workability of the concrete. Silica fume is thus widely used in SCC, especially for producing SCC with a high compressive strength.

Su et al. (2001) presented a calculation method to determine the mix proportion for SCC of a required compressive strength. The method considers the following as the major factors that influence the properties of SCC: the amounts of aggregates, binders and mixing water, and the type and dosage of superplasticizer (SP). Su et al. (2001) believed that the proposed method is simpler and easier for implementation and less time-consuming than the method of the Japanese Ready-Mixed Concrete Association (JRMCA), leading to a more economical design of SCC.

The use of fly ash is common in producing SCC and many studies have been concerned with the possible effect of using fly ash (e.g. Sonebi 2004). Sonebi (2004) found from his experimental results that for any given water-to-powder (W/P) ratio, an increase in the PFA (pulverized fuel ash, a type of fly ash) content led to a decrease in the compressive strength of SCC on the 7th and 28th days. Sonebi (2004) also concluded that SCC with a 28-day compressive strength of 30 to 35 MPa can still be achieved if the amount of PFA stays below $210 \text{ kg} / \text{m}^3$ of PFA.

2.2.3 Confined SCC

There has been rather limited research on the behavior of confined SCC. Lachemi et al. (2006) investigated the performance of axially loaded concrete-filled steel tube (CFST) columns cast using NC and SCC. The authors found that the casting of SCC was much less time-consuming than that of NC. CFST columns made with SCC could develop load capacities comparable to those made with NC. Both type of CFSTs showed good ductility and no significant difference in the corresponding axial strain at the ultimate axial stress. The confined strength of SCC, however, was found to be lower than that of NC.

In another independent study, Han and Yao (2004) found that when SCC was used in thin-walled hollow structural steel columns, the behavior of columns including the section capacity was similar to that of columns filled with NC.

El Chabib et al. (2005) presented the only study on the behavior of SCC confined in short GFRP tubes. The study used normal strength SCC and GFRP tubes with fiber angles of $\pm 55^\circ$. It was found from this study that the behavior of SCC-filled GFRP tubes was generally similar to that of NC-filled GFRP tubes under both uniaxial compression and transverse loading. However, there was also a significant difference between the behavior of SCC and that of NC-filled GFRP tubes: the stress-strain curves of the former showed a sudden shift from the linear portion to the nonlinear portion (i.e. after the unconfined strength of concrete was reached); such a sudden shift was not found or was not

pronounced in the stress-strain curves of the latter. El Chabib et al. (2005) believed that the sudden shift was due to the more severe shrinkage of SCC which produced a gap between the concrete and the GFRP FRP tube.

2.3 STRESS-STRAIN MODELS FOR FRP-CONFINED NORMAL CONCRETE

2.3.1 General

Many studies have been conducted in this area and numerous models have been proposed to predict the stress-strain curves of FRP-confined NC. The existing stress-strain models can generally be classified into two categories (Jiang and Teng 2007): (1) design-oriented models (e.g. Lam and Teng 2003) which are easy to apply in design and are generally in the form of closed-form equations directly derived from test results; and (2) analysis-oriented models (e.g. Jiang and Teng 2007) which treat the FRP jacket and the concrete core as separate components with their interactions considered through displacement compatibility and equilibrium conditions; analysis-oriented models can thus predict not only the axial stress-strain behavior, but also the lateral expansion behavior of the confined concrete. The present study focuses only on analysis-oriented models.

2.3.2 Analysis-oriented models

Jiang and Teng (2007) conducted a comparative study between existing analysis oriented models and a new model proposed by them (i.e. Jiang and Teng's model), and concluded

that their model, which was modified from the model originally proposed by Teng et al. (2007), was the most accurate model.

Jiang and Teng's (2007) model adopts the path-independence assumption, which implies that at a given axial strain, the axial stress and the lateral strain of the concrete confined with FRP are taken to be the same as those of the same concrete confined with a constant confining pressure (i.e. actively-confined concrete hereafter) equal to that provided by the FRP jacket. The model is composed of the following three elements: (1) an active-confinement base model which predicts the stress-strain curve of actively-confined concrete, (2) an axial strain-lateral/hoop strain relationship, and (3) a lateral strain-confining pressure relationship. These three elements of Jiang and Teng's (2007) model are briefly summarized below, and the reader may refer to Jiang and Teng (2007) for more details.

Active-Confinement Model

The active-confinement model adopted by Jiang and Teng (2007) can be expressed by the following equations.

$$\frac{\sigma_c}{f_{cc}^*} = \frac{(\varepsilon_c / \varepsilon_{cc}^*)^r}{r - 1 + (\varepsilon_c / \varepsilon_{cc}^*)^r} \quad (2.1)$$

$$r = \frac{E_c}{E_c - f_{cc}^* / \varepsilon_{cc}^*} \quad (2.2)$$

$$\frac{f_{cc}^*}{f_{co}'} = 1 + 3.5 \frac{\sigma_r}{f_{co}'} \quad (2.3)$$

$$\frac{\varepsilon_{cc}^*}{\varepsilon_{co}'} = 1 + 17.5 \left(\frac{\sigma_r}{f_{co}'} \right)^{1.2} \quad (2.4)$$

where σ_c and ε_c are the axial stress (MPa) and the axial strain of concrete respectively, E_c is the elastic modulus of concrete (MPa), σ_r is the confining pressure (MPa), f_{co}' is the cylinder compressive strength of unconfined concrete (MPa), ε_{co}' is the axial strain at the peak compressive stress of unconfined concrete (MPa), f_{cc}^* and ε_{cc}^* are respectively the peak axial stress (MPa) and the corresponding axial strain of concrete under a specific constant confining pressure.

Lateral Strain Equation

The following equation was adopted by Jiang and Teng (2007) for the axial strain-lateral/hoop strain relationship:

$$\frac{\varepsilon_c}{\varepsilon_{co}'} + 0.85 \left(1 + 8 \frac{\sigma_r}{f_{co}'} \right) \left\{ \left[1 + 0.75 \left(\frac{\varepsilon_l}{\varepsilon_{co}'} \right) \right]^{0.7} - \exp \left[-7 \left(\frac{\varepsilon_l}{\varepsilon_{co}'} \right) \right] \right\} = 0 \quad (2.5)$$

where ε_l is the lateral/hoop strain.

Confining Pressure

Based on force equilibrium, the confining pressure σ_l (MPa) can be related to the lateral/hoop strain ε_l by the following equation:

$$\sigma_l = -\frac{E_{frp} t_{frp} \varepsilon_l}{R} \quad (2.6)$$

where E_{frp} is the elastic modulus of FRP in the hoop direction of the FRP jacket (MPa), t_{frp} is the thickness of the FRP jacket (mm), and R is the radius of the confined concrete core (mm).

Because of the accuracy of Jiang and Teng's (2007) model and its capacity of predicting both the axial stress-strain behavior and the lateral expansion behavior of FRP-confined NC, this model was used to predict the behavior of FRP-confined NC in the present study. The predictions from Jiang and Teng's (2007) model are then compared with the experimental results obtained in the present study on SCC to clarify any difference between the FRP-confined NC and FRP-confined SCC.

2.4 PREDICTION OF THE MATERIAL PROPERTIES OF GFRP TUBES

The elastic properties of GFRP tubes may also be found using the lamination theory. Details of the lamination theory can be found in Section 2.6 Gibson (2012).

2.5 TESTING STANDARDS FOR FRP TUBES

In a typical concrete-filled FRP tubular column, the FRP tube is subjected to longitudinal compression and hoop tension. When the loading eccentricity is large or when bending is dominant, part of the FRP tube may also be subjected to tension in the longitudinal

direction. Therefore, existing testing standards for FRP tubes under hoop tension, longitudinal tension and compression are reviewed and summarized below.

2.5.1 Tensile coupon tests

ASTM D3039/D3039M (2000) is a widely used standard for determining the tensile properties of polymer matrix composite materials, including FRP. The recommendations of this standard for the geometry of tensile test coupon specimens are listed in Table 1 and Table 2 of the standard. The recommended testing speed is 2 mm/min.

ASTM D3039/D3039M (2000) suggests the following equation to be used for the calculation of tensile stress and tensile strength:

$$\begin{aligned} F^{tu} &= P^{\max} / A \\ \sigma_i &= P_i / A \end{aligned} \tag{2.9}$$

where

F^{tu} = ultimate tensile strength, MPa
 P^{\max} = maximum force before failure, N
 σ_i = tensile stress at i th data point, MPa
 A = average cross-sectional area, mm²

The calculation of tensile chord modulus of elasticity can be done using the following equation:

$$E^{chord} = \Delta\sigma / \Delta\varepsilon \tag{2.10}$$

where

- E^{chord} = tensile chord modulus of elasticity, GPa
 $\Delta\sigma$ = difference in applied tensile stress between the two strain points
as defined in Table 3 of ASTM D3039/D3039M, MPa
 $\Delta\varepsilon$ = difference between the two strain points of
as defined in Table 3 of ASTM D3039/D3039M

The Poisson's ratio can be calculated using the following equation:

$$v = -\Delta\varepsilon_t / \Delta\varepsilon_l \quad (2.11)$$

where:

- v = Poisson's ratio;
 $\Delta\varepsilon_t$ = difference in the corresponding lateral strain between the two
longitudinal strain points as defined in Table 3 of ASTM D3039/D3039M, $\mu\varepsilon$; and
 $\Delta\varepsilon_l$ = difference between the two
longitudinal strain points as defined in Table 3 of ASTM D3039/D3039M, $\mu\varepsilon$.

2.5.2 Split-disk tests

ASTM D2290 (2008) is the most widely used testing standard for obtaining the apparent hoop tensile strength of plastic or reinforced plastic pipes using the so-called split-disk test. Figure 2.1 and Figure 2.2 show the test fixture and test specimen recommended by ASTM D2290 (2008) respectively. It is suggested that reduced sections are included in the test specimen to control the failure location.

The following testing procedure was recommended by ASTM D2290 (2008):

- 1) Measure the minimum width of the reduced area(s) to the nearest 0.025 mm (0.001 in.).
- 2) Mount the specimen on the lubricated periphery of the test fixture, with the reduced

area(s) centered 50.8 ± 5.08 mm (2.0 ± 0.2 in.) away from the split in the disk.

- 3) Run the test at a constant speed between 0.1 and 0.5 ipm (inch per minute, equals 2.54 to 12.7 millimeter per minute).
- 4) Record the maximum load carried by the specimen during the test.

The apparent ultimate tensile stress of the specimen can be calculated using the following equation:

$$\sigma_a = P_b / 2A_m \quad (2.12)$$

where

σ_a = apparent ultimate tensile stress of the specimen, MPa (or psi),

P_b = maximum or breaking load, or both, N (or lbf),

A_m = minimum cross-sectional area of the two measurements, $d \times b$, mm^2 (or in.^2)

d = thickness at minimum area, mm (or in.),

b = width at minimum area, mm (or in.)

It should be noted that ASTM D2290 (2008) was designed only to obtain the apparent hoop tensile strength. In the present study, the testing method recommended by ASTM D2290 (2008) was adopted with some revisions to obtain the hoop tensile elastic modulus.

2.5.3 Axial compression tests

GB-5350 (2005) is the national standard of the People's Republic of China for determining the longitudinal compressive properties of fiber-reinforced thermosetting plastic composite pipes. This standard was designed for fiber reinforced thermosetting

resin pipes with a diameter of 50 to 100mm and a diameter-to-thickness ratio below 50. GB-5350 (2005) is the only standard found by the author that is available for such tests and was used in the present study as a reference.

Two types of test specimens are recommended in GB-5350 (2005): the end-strengthened specimen with a height of 60 mm and the non-strengthened specimen with a height of 30 mm. The recommended end-strengthened specimen is shown in Figure 2.3, in which D stands for the outer diameter, d stands for the inner diameter, t_0 stands for the end-strengthening thickness, l stands for the width of the end-strengthening section, L stands for the distance between the two end-strengthening sections, and H stands for the total specimen height. The recommended testing speed is 1 to 2 mm/min.

2.6 CONCLUSIONS

This chapter has provided a review of existing research relevant to the present study. A summary of existing test methods has also been given. It is clear that the existing knowledge provides an important basis for understanding the behavior of hybrid FRP-concrete tubular columns filled with SCC. It is also clear that the existing work on confined SCC, especially FRP-confined SCC, has been rather limited. Existing research has shown that the behavior of FRP-confined SCC may differ from that of FRP-confined NC, and a more comprehensive study is needed to further clarify such differences. In particular, in a tubular column, the significant shrinkage of SCC may present a problem

in terms of the confinement effectiveness of the FRP tube. In this connection, the use of an expansive admixture, which can compensate for the shrinkage of SCC, may be an effective way to achieve better confinement in hybrid FRP-SCC columns.

2.7 FIGURES

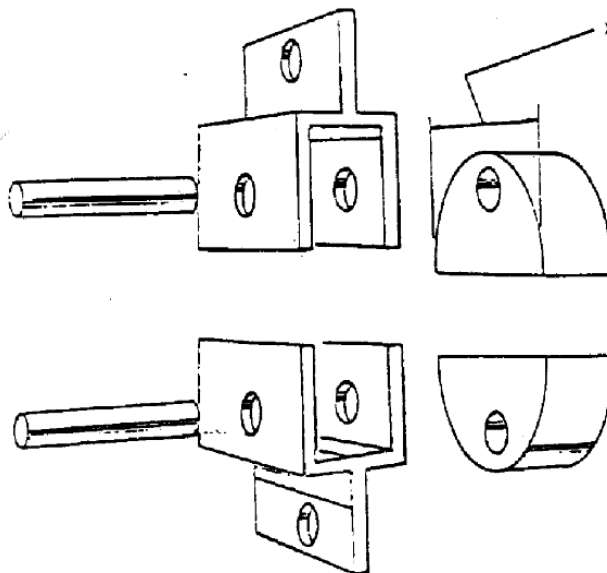


Figure 2.1 Typical test fixture of split-disk tests (Reproduced from ASTM D2290)

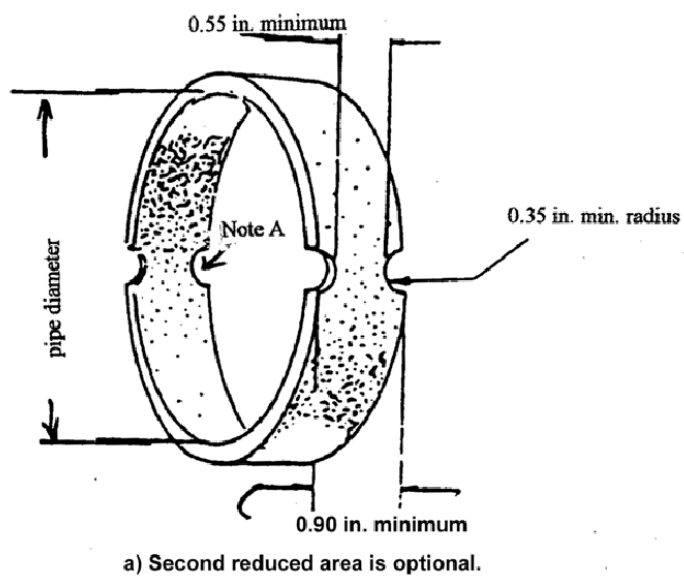


Figure 2.2 Typical split-disk test specimens (Reproduced from ASTM D2290)

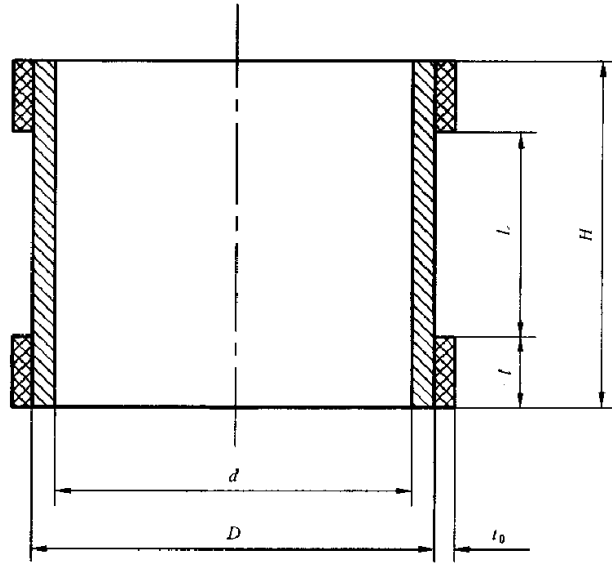


Figure 2.3 End-strengthened test specimens (Reproduced from GB 5350)

2.8 REFERENCES

- ASTM D2290. 2008. *Standard Test Method for Apparent Hoop Tensile Strength of Plastic or Reinforced Plastic Pipe by Split Disk Method*. American Society for Testing and Materials (ASTM), Philadelphia, USA.
- ASTM D3039/D3039M-00, 2000. *Standard Test Method for Tensile Properties of Polymer Matrix Composite Materials*, American Society for Testing and Materials (ASTM), Philadelphia, USA.
- BONEN, D. & SHAH, S. P. 2005. Fresh and hardened properties of self - consolidating concrete. *Progress in Structural Engineering and Materials*, Vol, 7, No. 1, pp. 14-26.
- DOMONE, P. 2007. A review of the hardened mechanical properties of self-compacting concrete. *Cement and Concrete Composites*, Vol. 29, No. 1, pp. 1-12.
- EL CHABIB, H., NEHDI, M. & EL NAGGAR, M. H. 2005. Behavior of SCC confined in short GFRP tubes. *Cement and Concrete Composites*, Vol. 27, No. 1, pp. 55-64.
- GB 5350. 2005. *Fiber-reinforced Thermosetting Plastic Composites Pipe-determination for Longitudinal Compressive Properties*. National Standard of People's Republic of China (GB), Beijing, China.
- GIBSON, R. F. 2012. *Principles of Composite Material Mechanics*, CRC press.
- HAN, L. H. & YAO, G. H. 2004. Experimental behaviour of thin-walled hollow structural steel (HSS) columns filled with self-consolidating concrete (SCC). *Thin-walled Structures*, Vol. 42, No. 9, pp. 1357-1377.

- JIANG, T. & TENG, J. G. 2007. Analysis-oriented stress–strain models for FRP–confined concrete. *Engineering Structures*, Vol. 29, No. 11, pp. 2968-2986.
- LACHEMI, M., HOSSAIN, K. M. A. & LAMBROS, V. B. 2006. Axial load behavior of self-consolidating concrete-filled steel tube columns in construction and service stages. *ACI Structural Journal*, Vol. 103, No. 1, pp. 38-47.
- LAM, L. & TENG, J. G. 2003. Design-oriented stress–strain model for FRP-confined concrete. *Construction and Building Materials*, Vol. 17, No. 6-7, pp. 471-489.
- MAZZOTTI, C., SAVOIA, M. & CECCOLI, C. Creep and shrinkage of self compacting concrete. 2nd FIB Conference, Proceeding of the 2nd International Congress, Naples, 2006. 1-10.
- PANESAR, D. & SHINDMAN, B. 2011. Elastic properties of self consolidating concrete. *Construction and Building Materials*, Vol. 25, No. 8, pp. 3334-3344.
- SONEBI, M. 2004. Medium strength self-compacting concrete containing fly ash: Modelling using factorial experimental plans. *Cement and Concrete research*, Vol. 34, No. 7, pp. 1199-1208.
- SU, N., HSU, K. C. & CHAI, H. W. 2001. A simple mix design method for self-compacting concrete. *Cement and Concrete Research*, Vol. 31, No. 12, pp. 1799-1807.
- TRAGARDH, J., 1999, Microstructural features and related properties of self-compacting concrete. *Proceedings of the First International RILEM Symposium on Self-Compacting Concrete*, pp. 175-186.

CHAPTER 3

AXIAL COMPRESSIVE BEHAVIOR OF SCC CONFINED BY AN FRP WRAP

3.1 INTRODUCTION

This chapter presents a series of axial compression tests aiming to clarify differences between FRP-confined NC and FRP-confined SCC. In the tests, FRP wraps with fibres oriented in the hoop direction only were used, so that the behaviour of the short columns was not complicated by the shrinkage of the SCC, and/or the significant axial stiffness and Poisson's effect of the FRP tube/wrap. The test variables included the material type and stiffness of FRP wraps and the concrete strength. This chapter first presents the experimental program and the test results from this study. The test results are then compared with the predictions of an accurate analysis-oriented stress-strain model developed by Jiang and Teng (2007) for FRP-confined NC to clarify any possible differences between the two types of confined concrete.

3.2 EXPERIMENTAL PROGRAM

3.2.1 Test specimens

As Jiang and Teng's (2007) model was developed based on a large amount of data of

FRP-confined NC cylinders and is able to represent the behavior of FRP-confined NC accurately, the present experimental study was concerned only with FRP-confined SCC cylinders. In total, 24 circular FRP-confined SCC cylinders (i.e. short circular columns) were prepared and tested in three series. Each series included four pairs of specimens covering four types of FRP jackets; the two specimens of each pair were nominally identical. The four different FRP jacket types were so designed that they covered three levels of confinement stiffness [see definitions by Jiang and Teng (2007)], with the lowest level corresponding to a stress-strain curve with a descending branch (i.e. weakly-confined concrete) and the other two levels leading to a continuously ascending stress-strain curve (i.e. sufficiently-confined concrete, including moderately-confined concrete and heavily-confined concrete). For one of the latter two levels, two types of FRP [i.e. carbon FRP (CFRP) and glass FRP or (GFRP)] were used to examine the effect of the hoop rupture strain of the FRP jacket. The SCC used in each series had the same unconfined concrete strength, but the concrete strengths were different for different series. The FRP jackets were formed via a wet-layup process with their finishing end overlapping their starting end by 150 mm. All specimens had a diameter of 152.5 mm and a height of 305 mm. All the specimens were strengthened at each end with a 25mm wide FRP strip (3-ply GFRP strips for GFRP-confined specimens and 2-ply CFRP strips for CFRP-confined specimens) to prevent local failure at the ends of the specimens. Other details of the specimens are summarized in the table below.

Table 3.1 Details of test specimens

Series	Specimen		Concrete strength			FRP	Confinement condition (W/M/H)
	Name	f'_{co} (MPa)	ϵ_{co} (%)	E_c (MPa)	$4730\sqrt{f'_{co}}$ (MPa)		
I	30C1-I,II	29.6	0.219	22.0×10^3	25.7×10^3	1-ply CFRP	M
	30C2-I, II	29.6	0.219	22.0×10^3	25.7×10^3	2-ply CFRP	H
	30G1-I, II	29.6	0.219	22.0×10^3	25.7×10^3	1-ply GFRP	W
	30G3-I, II	29.6	0.219	22.0×10^3	25.7×10^3	3-ply GFRP	M
	47C2-I, II	47.0	0.245	25.2×10^3	32.4×10^3	2-ply CFRP	M
II	47C3-I, II	47.0	0.245	25.2×10^3	32.4×10^3	3-ply CFRP	H
	47G3-I, II	47.0	0.245	25.2×10^3	32.4×10^3	3-ply GFRP	W
	47G6-I, II	47.0	0.245	25.2×10^3	32.4×10^3	6-ply GFRP	M
III	105C1-I, II	105	0.300	41.2×10^3	48.4×10^3	1-ply CFRP	W
	105C3-I, II	105	0.300	41.2×10^3	48.4×10^3	3-ply CFRP	M
	105C6-I, II	105	0.300	41.2×10^3	48.4×10^3	6-ply CFRP	H
	105G9-I, II	105	0.300	41.2×10^3	48.4×10^3	9-ply GFRP	M

It should be noted that in the confinement condition column of Table 3.1, “W” stands for a weakly-confined condition, “M” stands for a moderately-confined condition and “H” stands for a heavily-confined condition. Each specimen is named as follows (see Table 3.1): (a) a two- or three-digit number to represent the concrete strength; (b) a letter (“C” or “G”) to represent the type of FRP (i.e., CFRP or GFRP); (d) a single-digit number to define the number of plies in the FRP jacket; and (e) a Roman number to differentiate between the two nominally identical specimens. For example, specimen 30C2-II is the second specimen of a pair that had a two-ply CFRP jacket and a concrete cylinder compressive strength of 30MPa.

3.2.2 Mix design

A separate batch of SCC was prepared for each series of specimens. For the first two series, the concrete was prepared with ordinary Portland cement, fly ash, superplasticizer

(S.P.), river sand, and granite aggregate (agg.) with a maximum nominal size of 20 mm. In Series III, silica fume was added and the maximum aggregate size was reduced to 10 mm to achieve the high strength required. The mix proportions used are summarized in Table 3.2. For each series, three concrete cylinders ($152.5\text{mm} \times 305\text{mm}$) were tested to obtain the properties of the SCC following ASTM C469/C469M (2010). The average values of the elastic modulus, compressive strength (f'_{co}) and compressive strain at peak stress (ε_{co}) found from these tests are listed in Table 3.1. For comparison, the elastic moduli calculated from $E_c = 4730\sqrt{f'_{co}}$, which is the formula suggested by ACI (2008) for NC, are also listed in Table 3.1. The comparison shows that the elastic moduli of the SCC used in the present study are generally lower than those of the corresponding NC with the same strength. This observation agrees with that reported in Domone (2007) where a review of mechanical properties of SCC is presented.

Tensile tests of both CFRP and GFRP flat coupons were conducted following ASTM D3039/D3039M (2000). These tests showed that the GFRP used had an elastic modulus of 76 GPa and an ultimate stress of 1239 MPa based on a nominal thickness of 0.170 mm per ply, while the CFRP used had an elastic modulus of 222 GPa and an ultimate stress of 2494 MPa based on a nominal thickness of 0.166 mm.

Table 3.2 Mix design of SCC

	Series I	Series II	Series III
Water (kg/m ³)	198	167	166
S.P (liter/m ³)	3.00	6.00	16.0
Cement (kg/m ³)	239	309	420
Fly ash (kg/m ³)	204	206	185
Sand (kg/m ³)	722	727	750
10mm agg. (kg/m ³)	383	380	778
20mm agg. (kg/m ³)	575	570	0
Silica fume (kg/m ³)	0	0	67.2
Slump flow diameter (mm)	695	710	680

3.2.3 Test set-up and instrumentation

For each FRP-confined circular SCC cylinder, five pairs of strain gauges with a gauge length of 20 mm were installed at the mid-height of the FRP jacket. Each pair included one axial strain gauge and one hoop strain gauge. Among the five pairs of strain gauges, four (i.e. A~D) were evenly distributed around the circumference, including one that was placed at the middle of the overlapping zone. The fifth pair (i.e. E) was installed at the end of the overlapping zone where the hoop strain of FRP was expected to be higher than elsewhere (Chen et al. 2010). The circumferential layout of the strain gauges is shown in Figure 3.1 where the overlapping zone spans a circumferential distance of 150mm.

In addition, two linear variable displacement transducers (LVDTs) were used to obtain the axial deformation of mid-height region of the specimen because this region is least affected by end effects. The present compression tests were undertaken using an MTS machine and displacement control at a rate of 0.18 mm/min was adopted. The test data, including strains, loads, and displacements, were all recorded by a data logger

simultaneously. The test set-up is shown in Figure 3.2.

3.3 TEST RESULTS AND DISCUSSIONS

3.3.1 Test results

The general test results are listed in the following table.

Table 3.3 Key test results

Specimen	f'_{cc} (MPa)	$\frac{f'_{cc}}{f'_{co}}$	ε_{cu} (%)	$\frac{\varepsilon_{cu}}{\varepsilon_{co}}$	ε_{rup} (%)
30C1-I, II	41.4	1.40	1.00	4.60	0.860
	42.8	1.75	1.00	4.61	1.06
30C2-I, II	61.8	2.09	1.72	7.89	1.05
	59.7	2.02	1.45	6.62	1.02
30G1-I, II	31.0	1.05	1.29	5.90	1.59
	33.7	1.14	0.90	4.11	1.66
30G3-I, II	44.6	1.51	1.40	6.40	1.43
	44.9	1.52	1.47	6.71	1.59
47C2-I, II	69.6	1.48	0.95	3.86	0.90
	74.3	1.58	1.16	4.74	1.07
47C3-I, II	87.0	1.85	1.25	5.08	0.95
	87.0	1.85	1.24	5.04	0.90
47G3-I, II	52.6	1.12	1.00	4.06	1.48
	48.9	1.04	0.98	4.01	1.53
47G6-I, II	81.8	1.74	1.65	6.73	1.33
	85.5	1.82	1.65	6.73	1.45
105C1-I, II	116	1.11	0.84	2.80	0.97
	113	1.08	0.62	2.06	0.65
105C3-I, II	119	1.14	0.63	2.10	0.66
	121	1.16	0.83	2.76	0.63
105C6-I, II	190	1.82	1.35	4.50	1.05
	196	1.87	1.46	4.86	0.94
105G9-I, II	134	1.28	1.39	4.63	1.15
	152	1.45	1.40	4.67	1.25

The compressive strength of confined concrete f'_{cc} and ultimate axial strain ε_{cu} have been compared with the corresponding values for unconfined concrete f'_{co} and ε_{co} . The average hoop rupture strain for each specimen ε_{rup} is also reported in Table 3.3.

3.3.2 General behavior

All the test specimens failed due to the rupture of the FRP jacket which was subjected to hoop tension (Figure 3.3). As expected, the load kept increasing for the sufficiently-confined specimens in Series I and II, but decreased gradually or remained nearly constant in the later stage of deformation for the weakly-confined specimens (i.e. specimens 30G1 and 47G3) in these two series.

By contrast, the specimens in Series III showed quite different behavior because of the very high unconfined concrete strength of these specimens. Except for the two specimens with a very stiff FRP jacket (i.e. specimens 105C6-I, II with a 6 ply CFRP jacket) which still displayed a continuously ascending stress-strain curve, all the other specimens in this series experienced a sudden drop in the load shortly after the concrete had reached its unconfined strength. Rupture of the FRP jacket occurred soon after this sudden load drop for the two weakly-confined specimens (i.e. specimens 105C1-I, II), but for the other four specimens (i.e. specimens 105C3-I, II and 105G9-I, II), the load increased again until the occurrence of FRP rupture at a significantly larger axial strain.

3.3.3 Axial stress-strain behavior

The normalized axial stress-strain curves of all the 24 specimens are shown in Figure 3.4 while the key test results are summarized in Table 3.3. In Table 3.3, f'_{cc} is the peak axial stress of concrete, ε_{cu} is the ultimate axial strain, and ε_{rup} is the hoop tensile rupture

strain of FRP. In both Figure 3.4 and Table 3.3, f'_{cc} is normalized by the cylinder compressive strength f'_{co} , while ϵ_{cu} is normalized by ϵ_{co} , to highlight the effect of confinement from the FRP jacket. In the present study, unless otherwise specified, the axial stress was obtained by dividing the load resisted by the specimen by its cross-sectional area, the axial strain was calculated from the average reading of the two LVDTs, while the hoop strain of the FRP jacket was averaged from the readings of the three hoop strain gauges outside the overlapping zone (i.e. at points A-C in Figure 3.1). The following sign convention is adopted for stresses and strains in the concrete in this paper: compressive stresses and strains are positive while tensile stresses and strains are negative.

It is evident from Figure 3.4 that the two nominally identical specimens of each pair generally have very similar axial stress-strain curves except specimens 30G1-I, II and specimens 105C1-I, II. These two pairs of specimens are both weakly-confined specimens with a descending branch in the stress-strain curve, suggesting that a larger scatter of test results exists for such weakly-confined concrete.

All the sufficiently-confined specimens in Series I and II have an approximately bilinear axial stress-strain curve, which is similar to that of FRP-confined NC (Figure 3.4). For Series III whose concrete has a very high compressive strength (i.e. 105 MPa), the two specimens confined with a very stiff FRP jacket (i.e. 105C6-I, II) also have an approximately bilinear curve, but a significant drop in the stress occurs for the other four

sufficiently-confined specimens (i.e. 105C3-I, II and 105G9-I, II). For these four specimens, the axial stress increases again with the axial strain at an approximately constant rate (i.e. an approximately linear portion on the stress-strain curve) following the drop in the stress (Figure 3.4c).

It has been well established that the behavior of FRP-confined NC depends on the hoop stiffness of the FRP confining jacket. When all other parameters are the same, a stiffer FRP jacket leads to greater increases in strength and ductility. The stiffness of FRP jacket in general has similar effects on FRP-confined SCC as is evident from Table 3.3. This effect is also clear in Figure 3 where the stress-strain curves of specimens with a stiffer FRP jacket are seen to have a steeper second portion.

The effect of FRP rupture strain is also found to be similar to that in FRP-confined NC: if the confinement stiffness and the unconfined concrete strength are the same, a larger hoop rupture strain leads to a longer stress-strain curve which terminates at a larger peak stress and a larger ultimate axial strain. A good example of this effect can be observed in Figure 3.4 by comparing the results of specimens 30C1 with those of 30G3.

3.3.4 Axial strain-hoop strain relationship

It is now widely accepted that the relationship between axial strains and hoop strains of confined concrete is the key parameter that controls the effectiveness of FRP confinement

(Teng et al. 2007). This relationship has been investigated by many researchers for FRP-confined NC, but no such information is available for FRP-confined SCC. Figure 3.5 shows the axial strain-hoop strain curves of all 24 FRP-confined SCC specimens tested in the present study. As has been well established for FRP-confined NC, the SCC cylinders confined with a stiffer FRP jacket generally have lower curves, indicating that the lateral expansion of concrete depends significantly on the confinement stiffness: at the same axial strain, the larger the confinement stiffness, the less the lateral expansion of concrete.

3.3.5 Hoop rupture strains

Figure 3.6 shows the circumferential distributions of hoop strains of the mid-height section at the ultimate state of FRP rupture. The average hoop strains ε_{rup} at the ultimate state, which were found from the three hoop strains at points outside the overlapping zone (i.e. at points A, B, and C, see Figure 3.1) are generally similar to each other, and are generally significantly higher than those within or at the edge of the overlapping zone (i.e. at points D and E); this phenomenon has been observed by previous researchers (Lam and Teng, 2004) who attributed the lower hoop strains in the overlapping zone to the greater thickness of the FRP jacket there. It is interesting to note that for the Series III specimens which had high strength concrete (i.e. 105MPa), the average hoop rupture strains of specimens with a 6-ply CFRP jacket (i.e. specimens 105C6) are considerably higher than those of specimens with a 1-ply or a 3-ply CFRP jacket (see Figure 3.6c and

Table 3.3). The hoop strain distributions of the 1-ply and the 3-ply specimens are also more non-uniform. This phenomenon of specimens with high strength concrete is believed to be due to the more brittle nature of the concrete which produces more pronounced non-uniformity in lateral expansion after the concrete reaches its unconfined strength. When the CFRP jacket is thicker (i.e. with a larger stiffness), the concrete is more strongly confined and less prone to deformation localization, so the hoop rupture strain is likely to be larger.

3.4 COMPARISON WITH JIANG AND TENG'S (2007) MODEL

To provide a quantitative assessment of the differences in behavior between FRP-confined SCC and FRP-confined NC, the experimental results from the present study are compared with the predictions of Jiang and Teng (2007) analysis-oriented model. Jiang and Teng's (2007) model was proposed based on a large test database and has been shown by these authors (Lee and Hegemier, 2009, Liang et al., 2012) to provide close predictions of test results of FRP-confined NC, in terms of both the axial stress-strain curve and the axial strain-hoop strain curve. Details of the model are provided in Section 2.3.2 of this thesis.

The comparisons are shown in Figure 3.4 and Figure 3.5 respectively for the axial stress-strain curves and the axial strain-hoop strain curves. In obtaining the predictions, the

material properties presented earlier in this chapter were used and the predicted curves were terminated at a hoop strain equal to the average FRP rupture strain of the two nominally identical specimens of a pair. Figure 3.4 and Figure 3.5 show that the predictions agree reasonably closely with the test results, indicating that FRP-confined SCC generally behaves similarly to FRP-confined NC. However, it is also noted that Jiang and Teng's (2007) model appears to predict lower axial stress-strain curves and higher axial strain-hoop strain curves (i.e. a smaller hoop strain corresponding to the same axial strain). This observation suggests that the lateral expansion of FRP-confined SCC may be a little larger than that of NC with the same concrete strength and the same confining FRP jacket.

In order to further examine this issue, the results of specimens 47C2-I and 47C2-II are compared with the results of three FRP-confined NC specimens tested by Jiang and Teng (2007) in Figure 3.7. The three specimens were nominally identical and were named as specimens 46-48 in Jiang and Teng (2007). They had an unconfined concrete strength of 47.6 MPa and a corresponding compressive strain of 0.279%, which are both similar to the respective values of specimens 47C2-I and II, and were confined by an FRP jacket which is also very similar to that used for specimens 47C2-I and II. Figure 3.7a shows a comparison for the axial strain-hoop strain curves, where both strains are normalized by the corresponding compressive strain at the peak axial stress of unconfined concrete. It is evident from Figure 3.7a that the curves of the two SCC specimens are considerably

higher than those of the three NC specimens, which lie very close to the predictions of Jiang and Teng (2007)'s model. Figure 3.7b shows a comparison for the axial stress-strain curves, where the stresses and strains are normalized by the unconfined concrete strength and the corresponding compressive strain respectively. The curves of all the five specimens appear to be quite similar (Figure 3.7b). As a higher lateral strain generally means a larger confining pressure from the FRP jacket, Figure 3.7a and Figure 3.7b suggest that the axial stress of confined SCC is comparable to that of confined NC subjected to a lower confining pressure. The above observations suggest that: (1) at the same axial strain, the lateral expansion of FRP-confined SCC is larger, leading to a larger confining pressure; (2) at the same axial strain and the same confining pressure, the axial stress of confined SCC is smaller. The second observation agrees with the findings by Lachemi et al. (2006) for steel-confined SCC.

It should also be noted that El Chabib et al. (2005) found from their test results that the stress-strain curves of FRP-confined SCC are different from those of FRP-confined NC in the transition region of the curves: for their FRP-confined SCC cylinders, there seemed to be a short time lag between when the concrete core reached the unconfined strength and when the FRP jacket was mobilized; this time lag is believed to be due to a possible small gap between the FRP jacket and the concrete core. However, such differences were not observed in the present study. Further examination of El Chabib et al. (2005) test data revealed that this could be due to the different mix portions used in their study. In El

Chabib et al. (2005) tests, besides the fly ash and superplasticizer which were also used in the present study, a significant amount of ground granulated blast furnace slag (GBFS) and viscosity-modifying admixture (VMA) was also used to make SCC.

Figure 3.4 also shows that Jiang and Teng's (2007) model fails to predict the sudden drop on the axial stress-strain curves of the Series III specimens. This is contrary to Xiao et al. (2010) observation that Jiang and Teng's (2007) model provides close predictions for conventional concrete with similarly high strengths but without silica fume. It should be noted that besides the difference in the mix proportions of concrete (the exclusion of silica fume and the use of a smaller amount of S.P.), the FRP jackets used in Xiao et al. (2010) all had a stiffness larger than those of the six specimens which experienced a stress drop in the present study. The stress drop of the present FRP-confined high strength concrete specimens may therefore be due to one or a combination of the following reasons: (1) the use of SCC; (2) the use of silica fume; (3) the use of a relatively weak FRP jacket. As such differences have not been observed in specimens of Series I and II, it may be safe to conclude that it was not the unique properties of SCC which caused the sudden drop in axial stress-strain curves. Considering also the test observation of El Chabib et al. (2005) as discussed above, it may be concluded that the additional use of mineral admixtures (e.g. silica fume and GBFS) is a possible factor that affects the lateral expansion properties of concrete. Further research is needed to clarify this issue, and improvements to Jiang and Teng's (2007) model are necessary before its use can be extended to such

high strength concrete.

3.5 CONCLUSIONS

This chapter has presented the results of a series of axial compression tests on FRP-confined self-compacting concrete (SCC). The test results showed that the behavior of FRP-confined SCC is generally similar to that of FRP-confined normal concrete (NC); the unconfined concrete strength, the stiffness of the FRP jacket, and the hoop strain capacity of the FRP jacket all have a similar effect on behavior for these two types of confined concrete. Jiang and Teng's (2007) model, which was originally developed for FRP-confined NC, has been shown to provide reasonably close predictions for FRP-confined SCC, especially for the axial stress-strain curves of moderately confined normal strength SCC and heavily confined high strength SCC. Although the behavior of SCC under weak FRP confinement is not well predicted by Jiang and Teng's (2007) model, this is not a significant issue as such weak confinement is unlikely to arise in hybrid FRP-concrete tubular columns. The experimental results indicated that: (1) at the same axial strain, the lateral expansion of FRP-confined SCC is larger, leading to a larger confining pressure; (2) at the same axial strain and the same confining pressure, the axial stress of confined SCC is smaller. The combination of the two effects means that the axial stress-strain curves of FRP-confined SCC can be closely approximated by a stress-strain model developed for FRP-confined NC, but the relationship between the ultimate axial strain and the ultimate hoop rupture strain may need to be refined. This is an important

conclusion as it means that design rules developed for hybrid FRP-concrete tubular columns cast with NC can be assumed to be directly applicable to such members cast with SCC, and vice versa. In addition, it should be noted that the use of mineral admixtures (e.g. silica fume and GBFS) may influence the behavior of FRP-confined concrete, and some research is needed to ascertain the effect when or where such use makes this influence a significant issue.

3.6 FIGURES

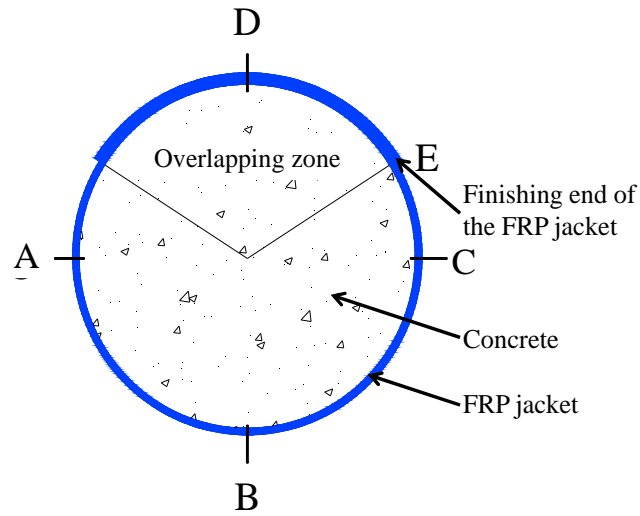


Figure 3.1 Layout of strain gauges

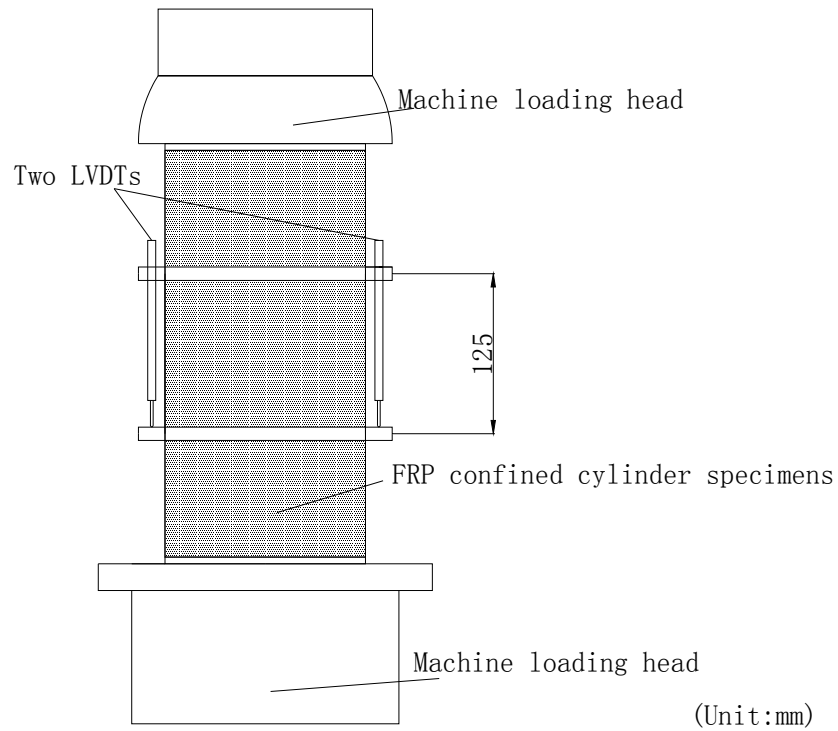
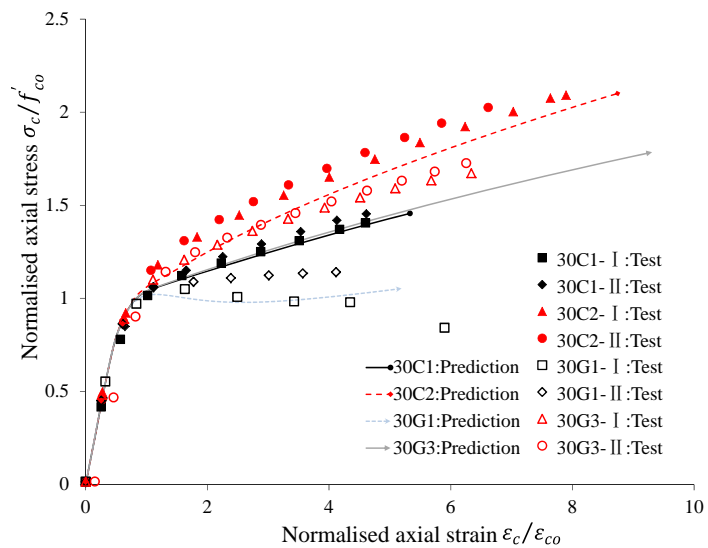


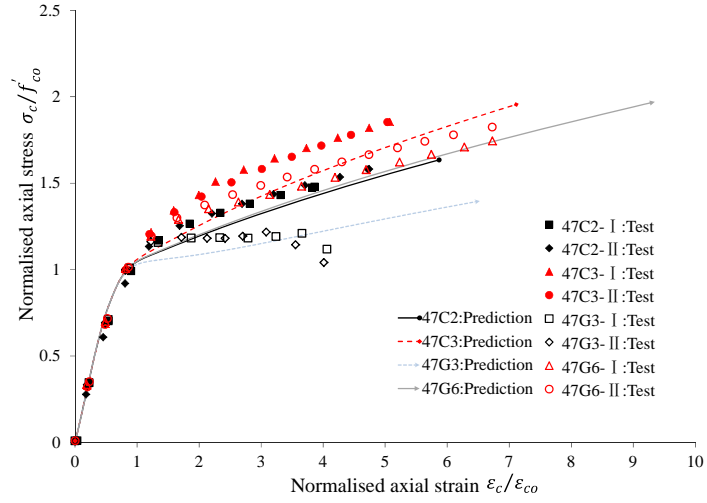
Figure 3.2 Test set-up



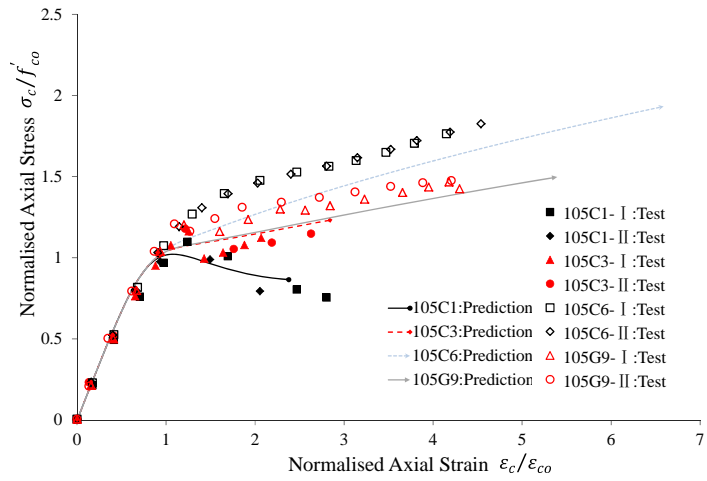
Figure 3.3 Typical failure mode of CFRP and GFRP jacket



(a) Series I

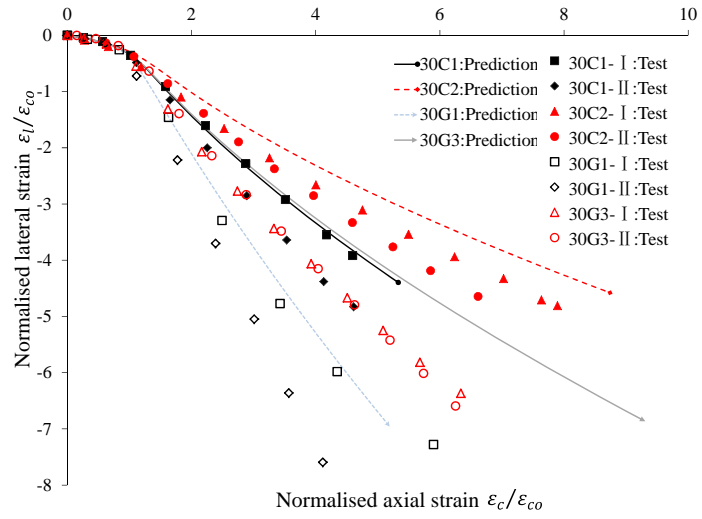


(b) Series II

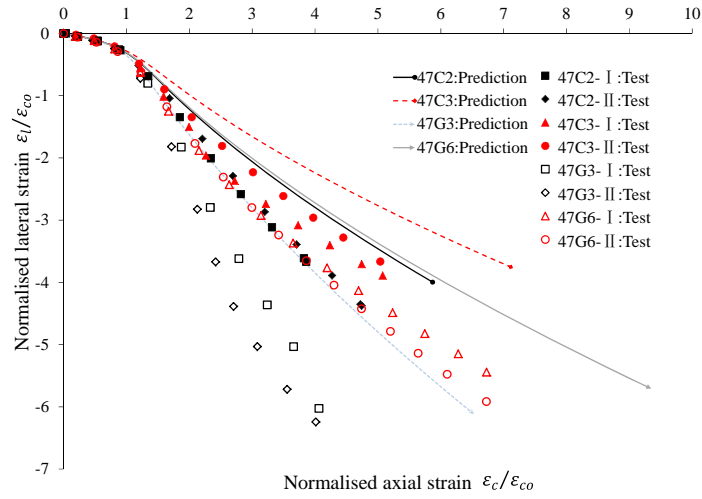


(c) Series III

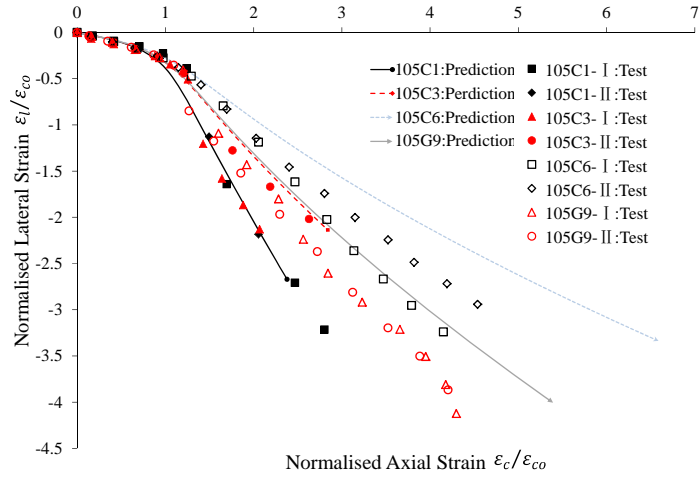
Figure 3.4 Axial stress-strain curves



(a) Series I

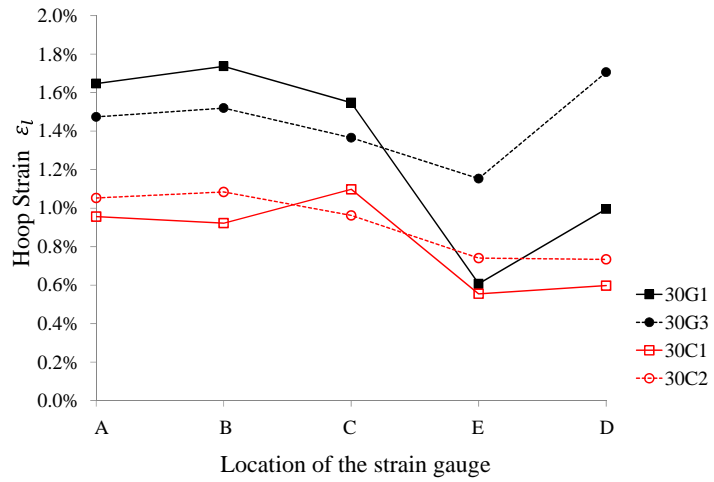


(b) Series II

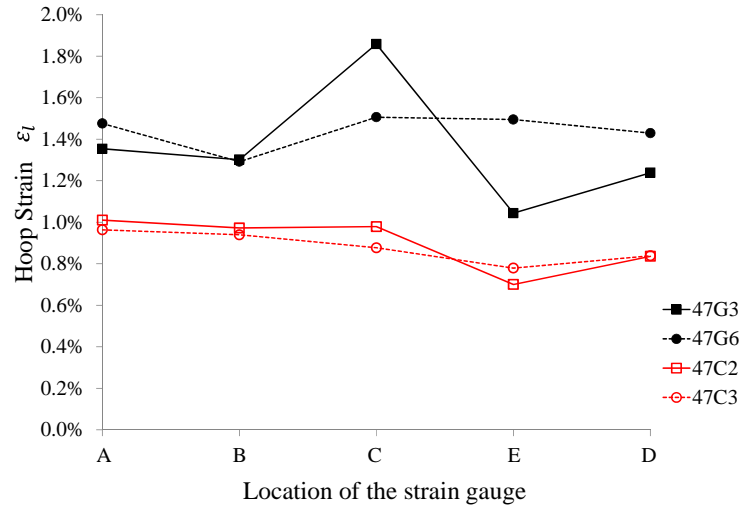


(c) Series III

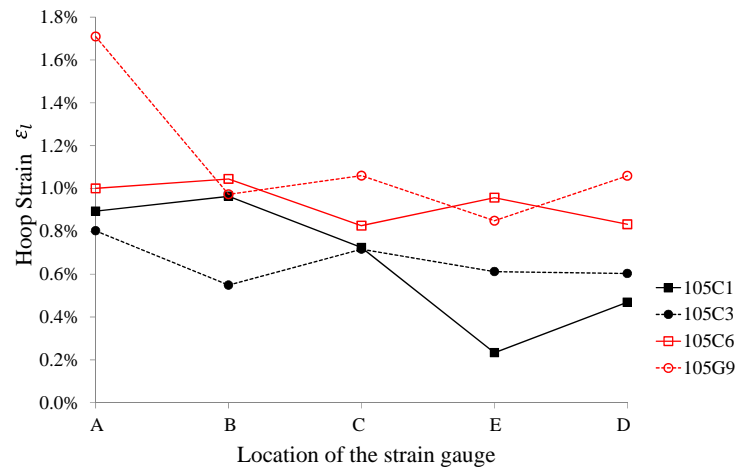
Figure 3.5 Axial strain-hoop strain curves



(a) Series I

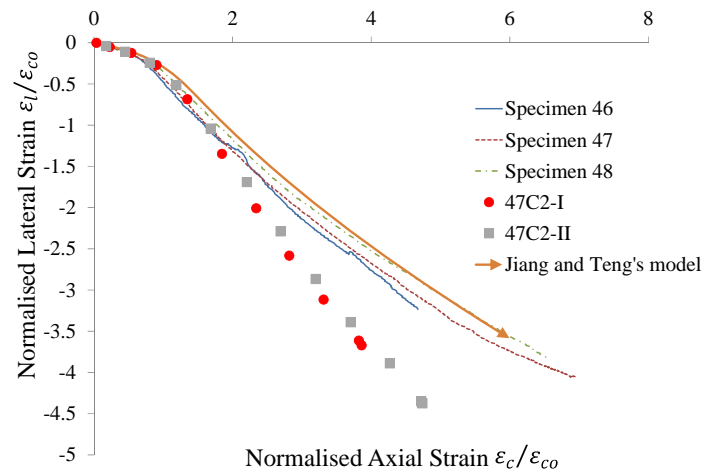


(b) Series II

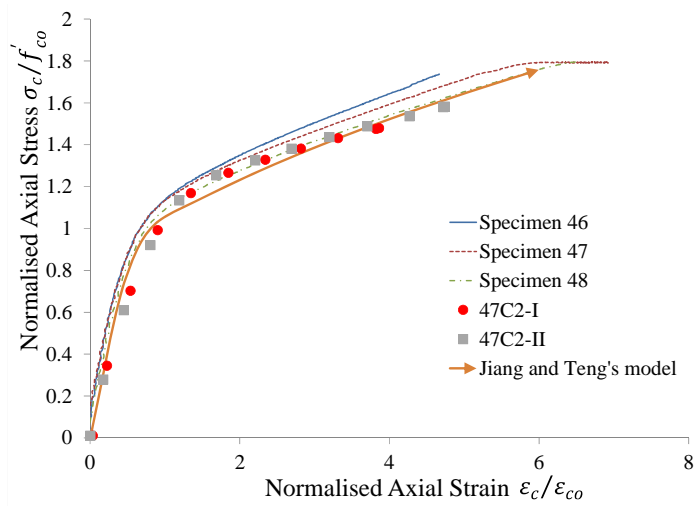


(c) Series III

Figure 3.6 Hoop rupture strain distribution around the circumference



(a) Axial strain-hoop strain curves



(b) Axial stress-strain curves

Figure 3.7 Comparison with Jiang and Teng's (2007) model

3.7 REFERENCES

- ASTM C469/C469M. 2010. *Standard Test Method for Static Modulus of Elasticity and Poisson'S Ratio of Concrete in Compression*, American Society for Testing and Materials (ASTM), Philadelphia, USA.
- ASTM D3039/D3039M-00. 2000. *Standard Test Method for Tensile Properties of Polymer Matrix Composite Materials*, American Society for Testing and Materials (ASTM), Philadelphia, USA.
- BONEN, D. & SHAH, S. P. 2005. Fresh and hardened properties of self - consolidating concrete. *Progress in Structural Engineering and Materials*, Vol. 7, No. 1, pp. 14-26.
- CHENG, L. & KARBHARI, V. M. 2006. New bridge systems using FRP composites and concrete: a state - of - the - art review. *Progress in Structural Engineering and Materials*, Vol. 8, No. 4, pp. 143-154.
- DOMONE, P. 2007. A review of the hardened mechanical properties of self-compacting concrete. *Cement and Concrete Composites*, Vol. 29, No. 1, pp. 1-12.
- EL CHABIB, H., NEHDI, M. & EL NAGGAR, M. H. 2005. Behavior of SCC confined in short GFRP tubes. *Cement and Concrete Composites*, Vol. 27, No. 1, pp. 55-64.
- FAM, A. Z. & RIZKALLA, S. H. 2001. Confinement model for axially loaded concrete confined by circular fiber-reinforced polymer tubes. *ACI Structural Journal*, Vol. 98, No. 4, pp. 451-461.
- HAN, L. H. & YAO, G. H. 2004. Experimental behaviour of thin-walled hollow structural

steel (HSS) columns filled with self-consolidating concrete (SCC). *Thin-walled structures*, Vol. 42, No. 9, pp. 1357-1377.

HAN, L. H., YAO, G. H. & ZHAO, X. L. 2005. Tests and calculations for hollow structural steel (HSS) stub columns filled with self-consolidating concrete (SCC). *Journal of Constructional Steel Research*, Vol. 61, No. 9, pp. 1241-1269.

HARRIES, K. A. & KHAREL, G. 2002. Behavior and modeling of concrete subject to variable confining pressure. *ACI Materials Journal*, Vol. 99, No. 2, pp. 180-189.

JIANG, T. & TENG, J. G. 2007. Analysis-oriented stress–strain models for FRP–confined concrete. *Engineering Structures*, Vol. 29, No. 11, pp. 2968-2986.

LACHEMI, M., HOSSAIN, K. M. A. & LAMBROS, V. B. 2006. Axial load behavior of self-consolidating concrete-filled steel tube columns in construction and service stages. *ACI Structural Journal*, Vol. 103, No. 1, pp. 38-47.

LAM, L. & TENG, J. G. 2002. Strength models for fiber-reinforced plastic-confined concrete. *Journal of Structural Engineering*, Vol. 128, No. 5, pp. 612-623.

LAM, L. & TENG, J. G. 2003. Design-oriented stress–strain model for FRP-confined concrete. *Construction and Building Materials*, Vol. 17, No. 6-7, pp. 471-489.

LAM, L. & TENG, J. G. 2004. Ultimate condition of fiber reinforced polymer-confined concrete. *Journal of Composites for Construction*, Vol. 8, No. 6, pp. 539-548.

LEE, C.-S. & HEGEMIER, G. A. 2009. Model of FRP-confined concrete cylinders in axial compression. *Journal of Composites for Construction*, Vol. 13, No. 5, pp. 442-454.

- LIANG, M., WU, Z.-M., UEDA, T., ZHENG, J.-J. & AKOGBE, R. 2012. Experiment and modeling on axial behavior of carbon fiber reinforced polymer confined concrete cylinders with different sizes. *Journal of Reinforced Plastics and Composites*, Vol. 31, No. 6, pp. 389-403.
- MIRMIRAN, A. 2003. Stay-in-place FRP form for concrete columns. *Advances in Structural Engineering*, Vol. 6, No. 3, pp. 231-241.
- MIRMIRAN, A. & SHAHAWY, M. 1997. Behavior of concrete columns confined by fiber composites. *Journal of Structural Engineering*, Vol. 123, No. 5, pp. 583-590.
- PAULTRE, P., KHAYAT, K. H., CUSSON, D. & TREMBLAY, S. 2005. Structural performance of self-consolidating concrete used in confined concrete columns. *ACI Structural Journal*, Vol. 102, No. 4, pp. 560-568.
- POPOVICS, S. 1973. A numerical approach to the complete stress-strain curve of concrete. *Cement and Concrete Research*, Vol. 3, No. 5, pp. 583-599.
- RICHART, F.E., BRANDTZAEG, A. & BROWN, R.L. 1928. A study of the failure of concrete under combined compressive stresses. *University of Illinois Bulletin*, 26, University of Illinois at Urbana-Champaign. Urbana, USA.
- TENG, J. G, HUANG, Y., LAM, L. & YE, L. 2007a. Theoretical model for fiber-reinforced polymer-confined concrete. *Journal of Composites for Construction*, Vol. 11, No. 2, pp. 201-210.
- TENG, J. G, YU, T., WONG, Y. L. & DONG, S. 2007b. Hybrid FRP–concrete–steel tubular columns: concept and behavior. *Construction and Building Materials*, Vol.

21, No. 4, pp. 846-854.

XIAO, Q. G., TENG, J. G., & YU, T. 2010. Behavior and modeling of confined high-strength concrete. *Journal of Composites for Construction*, Vol. 14, No. 3, pp. 249-259.

YU, T., TENG, J. G. & WONG, Y. L. 2010. Stress-strain behavior of concrete in hybrid FRP-concrete-steel double-skin tubular columns. *Journal of Structural Engineering*, Vol. 136, No. 4, pp. 379-389.

CHAPTER 4

AXIAL COMPRESSIVE BEHAVIOR OF SCC-FILLED GFRP TUBES

4.1 INTRODUCTION

Chapter 3 has presented a series of axial compression tests on circular SCC cylinders confined with an FRP wrap. In SCC-filled filament-wound FRP tubes, the behavior of the confined SCC is complicated by: (1) the possible shrinkage of SCC which may lead to a gap between the concrete and the confining tube; and (2) the more complicated mechanical behavior of the filament-wound FRP tube. A filament-wound FRP tube typically has fibers oriented at angles of non-zero degrees to both the longitudinal and the hoop directions. Such an FRP tube thus typically has a significant longitudinal stiffness, and it is more involved to obtain its mechanical properties in the two directions of concern (i.e. the longitudinal direction and the hoop directions) than an FRP wrap with all fibers oriented in the hoop direction.

This chapter presents a series of axial compression tests conducted on SCC-filled filament-wound FRP tubes. Prefabricated filament-wound tubes with fibers oriented at ± 80 degrees to the longitudinal axis were used. Associated material tests were conducted to obtain the material properties of the FRP tube in both the longitudinal and the hoop

directions. The main test variable was the amount of expansive admixture used in the SCC. The use of an expansive admixture was to compensate for the significant shrinkage of the SCC and to enable the concrete to be in intimate contact with the outer FRP tube. This chapter first presents the experimental program and the test results. Particular attention is placed on the mechanical properties of the FRP tubes. Jiang and Teng's (2007) stress-strain model is again used for comparison with the test results.

4.2 EXPERIMENTAL PROGRAM

4.2.1 Test specimens

In total, three pairs of SCC-filled GFRP tubes (see Table 4.1) were prepared and tested; each pair included two nominally identical specimens. The only difference between the three pairs of specimens was the percentage of expansive admixture used in the SCC. The expansive admixture was used in two of the three pairs of specimens to replace cementitious materials (i.e. cement and fly ash). All the GFRP tubes had the same inner diameter of 150 mm and the same height of 300 mm. The two ends of the column specimens were each strengthened with an additional two-ply CFRP strip (with a width of 25mm and a ply thickness of 0.17mm) to avoid local failure there. The concrete cylinder compressive strength was designed to be 84 MPa as the effect of shrinkage was believed to be more pronounced for higher strength concrete.

Table 4.1 Details of test specimens

Specimen	Percentage of expansive admixture (%)	Concrete property				GFRP tube fiber angle (°)
		f'_{co} (MPa)	ε_{co} (%)	E_c (MPa)	$4730\sqrt{f'_{co}}$ (MPa)	
84-0-I,II	0	83.6	0.293	35.3×10^3	43.2×10^3	
84-8-I,II	8	85.8	0.289	40.0×10^3	43.8×10^3	79.9
84-12-I,II	12	84.9	0.264	36.3×10^3	43.6×10^3	

Each of the test specimens is named as follows: (a) the first two-digit number represents the designed concrete strength of 84 MPa; (b) the second number indicates the percentage of expansive admixture; and (c) the Roman number differentiates between the two nominally identical specimens (i.e., I and II).

4.2.2 Mix design and properties of SCC

The relevant Chinese standard (GB-J119 1988) was used as a reference in the mix design. According to this standard, the suggested amount of expansive admixture is 8% to 12% of the cementitious materials (i.e. cement and fly ash). Therefore, 8% and 12% were chosen for two of the three pairs of specimens. The purpose of using an expansive admixture in the SCC is to compensate for the shrinkage of SCC and even to create possible initial lateral expansion of the concrete. The most commonly used expansive admixture (i.e. the ettringite type, see Nagataki and Gomi. 1998) was used in this study. Silica fume was also used to produce the high strength concrete according to Detwiler and Mehta (1989). Details of the mix proportions are summarized in

Table 4.2.

Concrete strength (MPa)- content of expansive admixture(%)	84-0	84-8	84-12
Water (kg/m ³)	158	158	158
Expansive admixture (kg/m ³)	0	48.4	72.6
Superplasticizer (liter/m ³)	13.0	13.0	13.0
Cement (kg/m ³)	420	387	370
Fly ash (kg/m ³)	185	170	163
Silica fume (kg/m ³)	67.2	67.2	67.2
Sand (kg/m ³)	752	752	752
10mm aggregate (kg/m ³)	782	782	782
Slump flow diameter (mm)	700	685	690

For each series, three standard concrete cylinders (152.5 mm x 305 mm) were tested to obtain the properties of the SCC. The average values of the elastic modulus E_c , compressive strength f'_{co} , and compressive strain at corresponding peak stress ϵ_{co} gained from tests are listed in Table 4.1. For comparison, the elastic moduli calculated using $E_c = 4730\sqrt{f'_{co}}$, which is the formula suggested by ACI (2008) for NC, are also listed in Table 4.1. It is clear from Table 4.1 that the elastic moduli of the SCC are lower than the corresponding values calculated by the formula which is accurate for NC. This finding is similar to that reported by Domone (2007). It is also clear that the use of an expansive admixture does not appear to affect much the resulting concrete strength.

4.2.3 Properties of GFRP tubes

All the specimens had the same type of filament-wound GFRP tubes with a thickness of

3.5 mm. According to the manufacturer, the volume ratio and the angles of the fibres in these tubes were 0.568 and ± 79.9 degrees to the longitudinal axis of the tube respectively.

In a separate PhD study conducted by Mr. Zhang Bing from the author's research group, filament-wound GFRP tubes with the same volume ratio and fiber angles were used. Therefore, the tubes used in Mr. Zhang Bing's study are assumed to have the same material properties as those of the present study, although they had different dimensions (i.e. diameter and thickness). The author worked together with Mr. Zhang to obtain the material properties of these GFRP tubes. Only selected tubes were tested under hoop tension and axial compression respectively.

As reviewed in Chapter 2, ASTM D2290 (2008) provides a test procedure for obtaining the apparent hoop tensile strength of FRP tubes using split-disk tests. The test procedure was revised to obtain the hoop elastic modulus of FRP tubes. Basically the test fixture and test specimen (Figure 2.1 and Figure 2.2) recommended by ASTM D2290 (2008) were adopted except that no reduced section was used in the test specimens. Six hoop strain gauges with a gauge length of 20 mm were installed on each specimen, among which two were located at the ends of the gap between the two half disks (Figure 2.1), while the other four were located at 15 mm away from the two ends of the gap. The strain gauges at the gaps were found to record lower strains as expected because of the effect of local bending there. The distance of 15 mm from the gaps for the remaining four strain

gauges was determined by a finite element analysis which indicates that this distance is sufficient to ensure that the effect of local bending is minor. Readings from the four strain gauges were used to obtain the hoop elastic modulus of the tubes.

In total, tensile split-disk tests on 10 FRP rings with a uniform height of 35 mm were conducted. 5 of the 10 rings were cut from the same FRP tube with a diameter of 200 mm and a thickness of 4.7 mm, while the other 5 were cut from an FRP tube with a diameter of 300 mm and a thickness of 6 mm. The experimental tensile stress-strain curves are shown in Figures 4.1 to 4.3, where the tensile stress was obtained by dividing the applied tensile force by two times the cross-sectional area of the ring, while the tensile strain was averaged from the four hoop strain gauges away from the gaps. Figure 4.1 to Figure 4.3 show that the FRP tube has a linear stress-strain relationship in the hoop direction. For the 200 mm tubes, the average rupture strain and secant elastic modulus at failure are 1.486% and 45.9 GPa, respectively. For the 300 mm tubes, the average rupture strain and secant elastic modulus at failure are 1.554% and 43.6 GPa, respectively. The failure mode of the ring specimens is shown in Figure 4.4 and Figure 4.5.

GB-5350 (2005) provides a test procedure to obtain the compressive properties of FRP tubes. This test procedure was adopted in the present study, with some modifications to the test specimens. In total 5 FRP rings were tested under axial compression. The 5 FRP rings all had a height of 60 mm and were cut from the same FRP tube with a thickness of

9.5 mm. It should be noted that the height of 60 mm was used in these tests instead of 30 mm recommended by GB-5350 (2005) in order to facilitate the installation of axial strain gauges. The use of a higher specimen was not expected to cause any buckling of these tubes because of their relatively large thickness. Four pairs of cross strain gauges, 90° apart from each other, were installed on each specimen to measure both axial and hoop strains. The tubes were tested on an MTS machine with a displacement control rate of 0.036 mm/min. Figure 4.6 shows the experimental stress-strain curves, while the failure mode of the specimens is shown in Figure 4.7. The stress is seen to increase linearly with the strain until an axial strain of around 0.004, after which the FRP tube exhibited significantly nonlinear behavior before the final failure of the tube due mainly to failure of the resin matrix. The average secant elastic modulus at an axial strain of 0.004, which represents the slope of the initial approximately linear portion, was found to be 15.6 GPa and was referred to as $E_{\text{sec},1}$. The average ultimate axial stress, axial strain and secant elastic modulus at failure (referred to as $E_{\text{sec},2}$) are 95.1 MPa, 0.95% and 10.0 GPa respectively.

The lamination theory summarized by Gibson (2012) was also used to calculate the elastic modulus in the hoop direction. The calculated elastic modulus is 40.8 GPa, which is close to the value obtained from the split-disk tests. Later work on the split disk test at PolyU indicated that the split disk test may lead to a small overestimate of the elastic modulus of a GFRP tube (Zhang 2014).

4.2.4 Test set-up and instrumentation

For each SCC-filled GFRP tube, eight groups of strain gauges with a gauge length of 20 mm were installed at the mid-height of the GFRP tube. Each group included three independent strain gauges: one axial strain gauge, one hoop strain gauge and one strain gauge at 45 degrees to both of the other two strain gauges. The eight groups of strain gauges were evenly distributed around the circumference. The circumferential layout of the strain gauges is shown in Figure 4.8.

In order to measure the axial shortenings of the 125 mm mid-height region of the specimen, two linear variable displacement transducers (LVDTs) were additionally installed. The present compression tests were undertaken using an MTS machine and displacement control at a rate of 0.18 mm/min was adopted. The test data, including strains, loads, and displacements, were all recorded by a data logger simultaneously.

4.3 TEST RESULTS AND DISCUSSIONS

4.3.1 Expansion of SCC

The lateral deformation of the six specimens was monitored for 3 days right after concrete casting to understand the possible expansion/shrinkage of the concrete. Readings from the lateral strain gauges of groups 1 and 5 (see Figure 4.8) were taken for this purpose.

Figure 4.9 to Figure 4.11 show the variations of hoop strains (only the readings from the

strain gauges) with time, and Figure 4.12 shows the specimens in the process of monitoring. While it is evident that there is a large scatter in the strain gauge readings, Figure 4.9 shows clearly that shrinkage occurred in the specimens with SCC without expansive admixture. Figure 4.10 and Figure 4.11, on the other hand, show that such shrinkage was compensated for with the addition of expansive admixture as the hoop strain became tensile 48 hours after the casting of concrete; for the specimens with the 12% expansive admixture, lateral expansion was found to occur.

4.3.2 General behavior

The specimens all failed by the rupture of the GFRP tube along the fiber directions due to the lateral expansion of concrete (see Figure 4.13 to Figure 4.15). The axial load kept increasing continuously for the specimens with expansive admixture (i.e. specimens 84-8-I, II and 84-12-I, II). For the group of specimens without expansive admixture, different responses were observed for the two nominally identical specimens: a drop in the axial load was found during the loading process of specimen 84-0-I, but such a load drop did not occur for specimen 84-0-II.

4.3.3 Axial load-strain relationship

Two ways for obtaining the axial strain of a specimen are available. One is to find the axial strain as the average of the readings from the two mid-height axial strain gauges,

while the other is to take it as the average of the readings from the two LVDTs. The axial strains from both methods were found to be very similar for all the specimens except for specimen 84-12-I where one of the LVDTs did not work properly (see Figure 4.16). In this chapter, unless otherwise specified, the axial strains refer to those obtained from the readings of the two LVDTs except for specimen 84-12-I for which the axial strain readings are used.

Figure 4.17 shows that the axial load-displacement curves of all the specimens. For comparison, the axial loads taken by the GFRP tubes are also shown in Figure 4.17, while the method of obtaining these axial loads is explained in the next section. It is evident that the curves of the two nominally identical specimens of the 84-12 pair and the 84-8 pair (i.e. the two pairs with expansive admixture) agree very well with each other. On the contrary, the two specimens with normal SCC (i.e. specimens 84-0-I and 84-0-II) behaved quite differently in the second stage of loading. The curve of specimen 84-0-II, different from all the other curves, has a sudden drop in the load at the beginning of the second portion. While it is not clear why the two nominally identical specimens showed different responses, the observation from specimen 84-0-II revealed that the significant shrinkage of SCC can be a potential problem in SCC-filled GFRP tube columns, and may result in a substantial reduction in both the axial strength and ductility of the column.

4.3.4 Axial stress-strain behavior

The axial stress of the concrete in the specimens is defined as the load resisted by the concrete section divided by its cross-sectional area. The load taken by the concrete is found as the load taken by the specimen subtracted by the load taken by the FRP tube at the same axial strain. The load carried by the FRP tube was obtained by making use of the results of the axial compression tests on the GFRP tubes, as explained below.

Calculation of the tube contribution to the axial load

Results from the axial compression tests on the five GFRP rings agree well with each other (Figure 4.6). The following equations were developed based on a regression analysis of the curves shown in Figure 4.6.

When $\varepsilon_{axial} \leq \varepsilon_{frp,o}$

$$\text{FrpStress(MPa)} = -961044 \times \varepsilon_{axial}^2 + 19129 \times \varepsilon_{axial} - 0.2463; \quad (4.1)$$

When $\varepsilon_{axial} \geq \varepsilon_{frp,o}$

$$\text{FrpStress(MPa)} = \sigma_{ultimate} \text{ (MPa)}$$

In the above equations, ε_{axial} stands for the axial strain, while $\sigma_{ultimate}$ and $\varepsilon_{frp,o}$ stand for the ultimate axial stress and the hoop strain of GFRP tube at ultimate axial stress (ε_{axial} and $\varepsilon_{frp,o}$ are in $\mu\varepsilon$) respectively. It should be noted that when the axial strain exceeds ε_{frp} of the corresponding hollow FRP tube test, it is assumed that the stress resisted by the FRP tube is equal to its ultimate stress. This assumption was made based on the fact

that inward buckling deformations of the FRP tube were prevented by the inner concrete core in an SCC-filled FRP tube. Apparently, this assumption may lead to overestimation of the load taken by the FRP tube, but such overestimation is believed to have only small effects on the resulting axial stress-strain curve of the concrete, as further illustrated later.

Equation 4.1 was thus used to obtain the axial load taken by the FRP tube in an SCC-filled FRP tube column.

Axial stress-strain behavior of SCC in SCC-filled GFRP tubes

Figure 4.18 shows the stress-strain curves of the confined SCC for all the test specimens while the key test results are summarized in Table 4.3. In Table 4.3, f'_{cc} is the peak axial stress of concrete, ε_{cu} is the ultimate axial strain and ε_{rup} is the hoop rupture strain of GFRP tube filled with SCC. The axial stress σ_c is nominalized by the unconfined concrete strength f'_{co} , and both the axial strain ε_{cu} and lateral strain ε_l (equal to the hoop strain) are nominalized by the axial strain of unconfined concrete ε_{co} at f'_{co} .

Table 4.3 Key test results of SCC-filled FRP tubes

Specimen	f'_{cc} (MPa)	$\frac{f'_{cc}}{f'_{co}}$	ε_{cu} (%)	$\frac{\varepsilon_{cu}}{\varepsilon_{co}}$	ε_{rup} (%)
84-0-I,II	117	1.40	0.96	3.38	1.00
	137	1.64	1.39	4.91	1.48
84-8-I,II	145	1.69	1.68	5.89	1.35
	138	1.61	1.16	4.07	1.20
84-12-I,II	140	1.65	1.68	5.92	1.29
	135	1.59	1.46	5.14	1.30

It is evident from Figure 4.18 that the confined SCC stress-strain curves of all the specimens with expansive mixture have a bilinear shape which is similar to that of SCC confined with an FRP wrap (see Chapter 3). The two nominally identical specimens of each pair have similarly axial stress-strain curves except specimens 84-0-I and 84-0-II. The stress-strain curve of specimen 84-0-I has a drop in the axial stress at the beginning of the second stage, and the specimen also failed at a lower ultimate axial strain. This is believed to be a result of the significant shrinkage of the SCC as discussed earlier. It should be noted that the SCC used in the tests presented in Chapter 3 also did not include an expansive admixture, but the shrinkage of concrete did not seem to cause a problem there. This is because in those tests, FRP wraps with unidirectional fibres were used and they were applied after the hardening of concrete when most of the shrinkage of SCC had been developed.

It may also be noted from Figure 4.18 that with an increase in the amount of expansive admixture, the second stage of the lateral stress-strain relationship tends to become more linear. This phenomenon indicates that the addition of expansive admixture leads to better confinement in SCC-filled GFRP tubular columns. From the results in Table 4.3, there is no indication that an increase in the amount of expansive admixture would lead to an increase in the ultimate stress. The ductility of the SCC-filled GFRP tubes, however, seems to be improved by the inclusion of an expansive admixture, as shown in Table 4.3.

Predictions from Jiang and Teng (2007) analysis-oriented model are compared with the test results in Figure 4.18. In making the predictions, an important parameter is the hoop elastic modulus of the FRP E_{frp} . The fibers in filament-wound GFRP tubes are not unidirectional and they are oriented at some angles to the hoop direction. The equivalent elastic modulus in the hoop direction can be calculated using the lamination theory or through the split-disk test. In the present study, both methods were used and the results appear to be similar. As ring split disk tests were not conducted directly for the 150 mm GFRP tubes used in the present column tests and such split disk tests may overestimate the hoop elastic modulus of GFRP tubes, the result from the lamination theory was used in the analysis; that is, E_{frp} is taken to be 40.8 GPa.

Figure 4.18 shows that Jiang and Teng's (2007) model provides reasonable predictions, but overestimates significantly the ultimate axial stress and the ultimate axial strain of all the specimens. In addition, Jiang and Teng's (2007) model cannot predict the sudden drop in the stress-strain curve of specimen 84-0-II, which is believed to be caused by the shrinkage of SCC.

As discussed earlier, the derivation of the load taken by the GFRP tube from the total load taken by the column may introduce some errors in obtaining the stress-strain curves of the confined SCC. The load taken by the GFRP tube is generally small, being below 8% of the total load taken by the column when the column is at the maximum load. Therefore,

any errors arising from the inaccurate account of the GFRP tube contribution are believed to have only small effects on the stress-strain curves shown in Figure 4.19 and Figure 4.20.

4.3.5 Axial strain-hoop strain relationship

The axial strain-lateral strain relationship of confined concrete is the key element that determines the effectiveness of FRP confinement (Teng et al., 2007). Figure 4.21 shows the axial strain-hoop strain relationship of each specimen, where the hoop strains were averaged from readings of the 8 hoop strain gauges. Predictions from Jiang and Teng's (2007) model are also shown in Figure 4.21 for comparison and are found to be generally higher than the experimental curves, indicating that this model tends to predict a higher axial strain at the same hoop strain. The difference between the predicted curve and the experimental curves appears to be more pronounced for the specimen without any expansive admixture.

4.4 HOOP RUPTURE STRAINS

Figure 4.22 shows the distributions of hoop strains at the ultimate state for all the specimens. The hoop strains are those at the mid-height section of the specimens recorded by 8 strain gauges (see Figure 4.8). The No.7 strain gauge of specimen 84-8-II malfunctioned during the test and no valid data were recorded by this strain gauge.

Therefore, it is excluded from the figures. From the results of Figure 4.22, it is clear that with an increase in the amount of expansive admixture, the hoop strain distribution trends to be more even.

4.5 CONCLUSIONS

This chapter has presented the results of a series of axial compression tests on SCC-filled GFRP tubes and associated material tests for the GFRP tubes. The test results show that the use of a suitable amount of expansive admixture can compensate for the excessive shrinkage of SCC and thus enhance the performance of the column. It is therefore recommended that an expansive admixture should be included in SCC in constructing SCC-filled GFRP tubular columns in practice, following appropriate guidelines/standards. Jiang and Teng's (2007) analysis-oriented stress-strain model, which was developed for FRP-confined NC, has been shown to provide reasonable predictions for the axial stress-strain response of SCC confined by a filament-wound GFRP tube with fibers close to the hoop direction. This model, however, appears to significantly overestimate the axial strain for a given hoop strain. As a result, the model also significantly overestimates the ultimate axial stress and the ultimate axial strain of such concrete. Research is needed to identify possible refinements to this model when more test data become available.

4.6 FIGURES

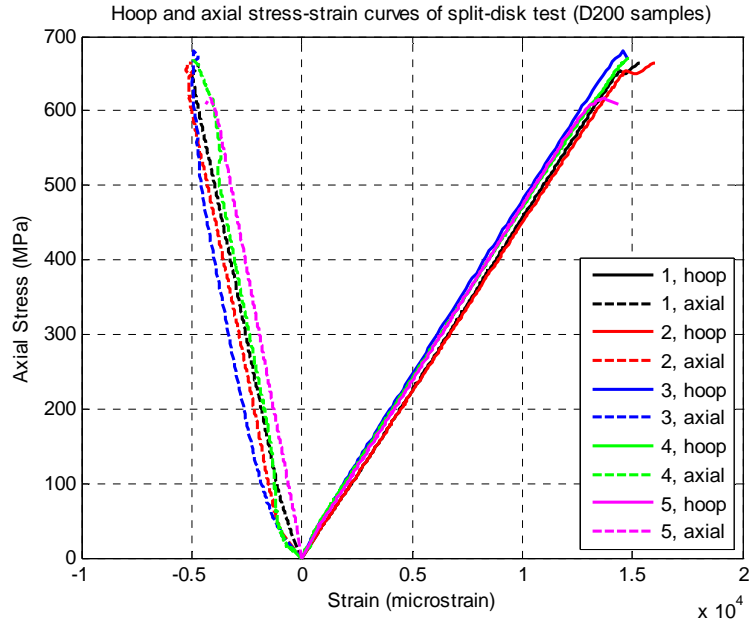


Figure 4.1 Hoop and axial stress-strain curves from split-disk tests for D200 specimens

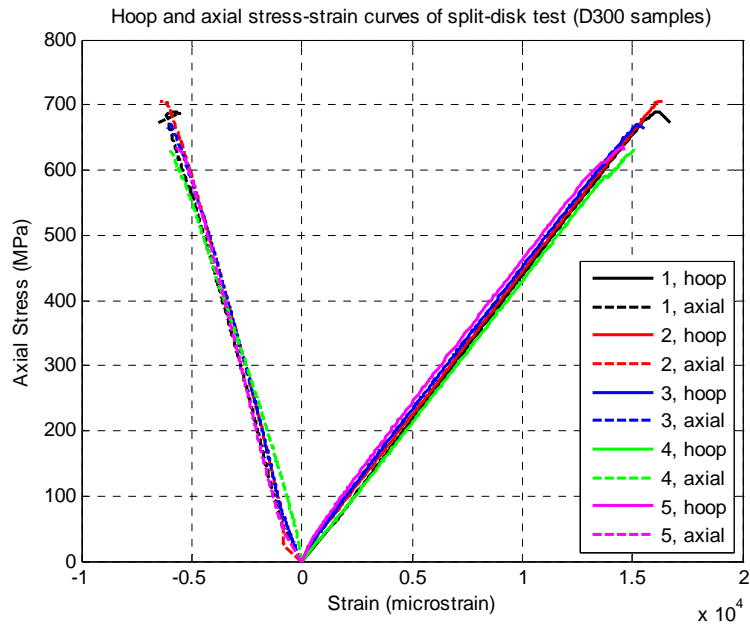


Figure 4.2 Hoop and axial stress-strain curves from split-disk tests for D300 specimens

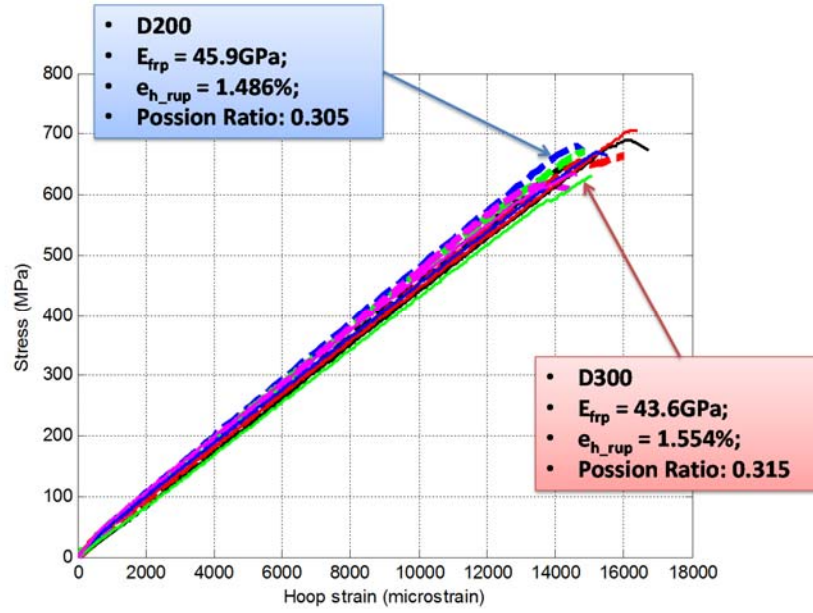


Figure 4.3 Hoop stress-strain curves from split-disk tests of specimens with fiber angles of ± 80 degrees with the diameters of 200mm and 300mm

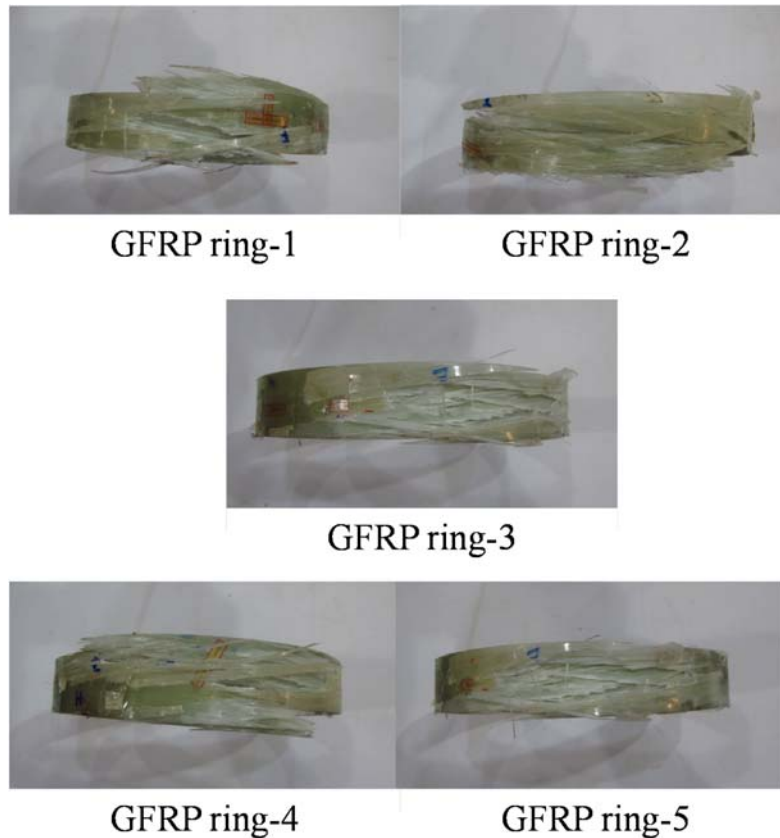


Figure 4.4 Failure mode of split-disk test specimens (D200 specimens)

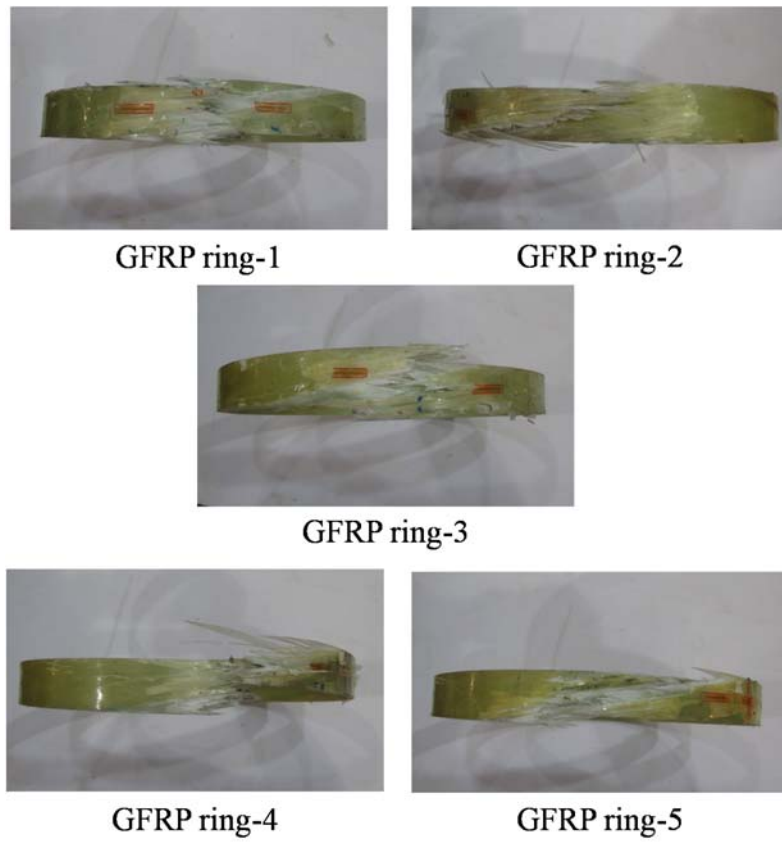


Figure 4.5 Failure mode of split-disk test specimens (D300 specimens)

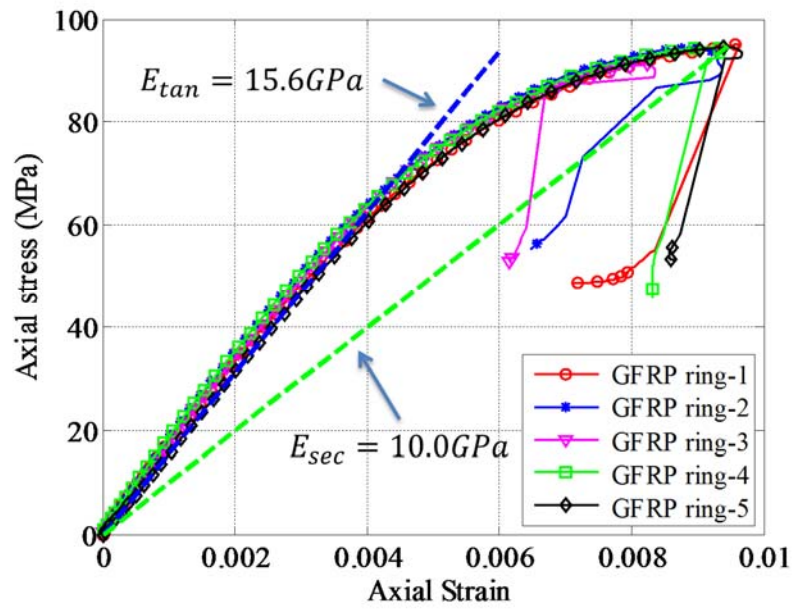
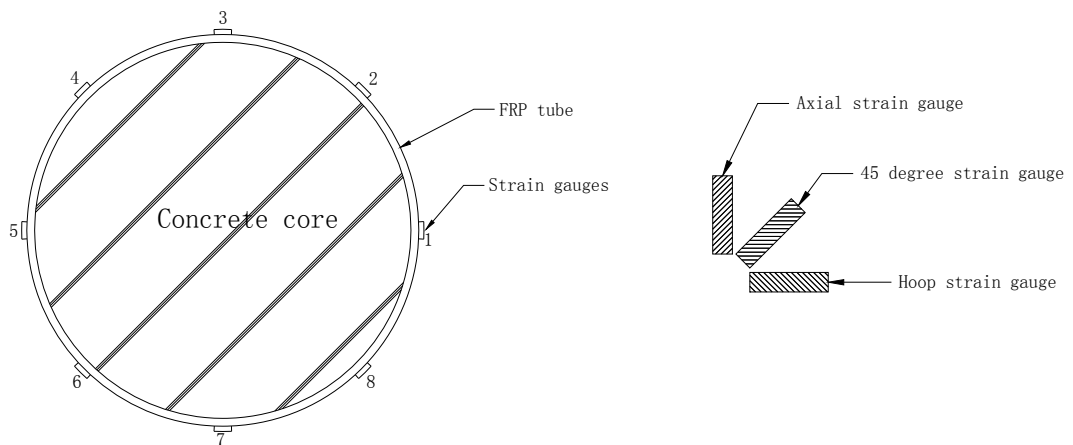


Figure 4.6 Axial stress-strain curves of the D200 specimens tested by Mr. Zhang Bing

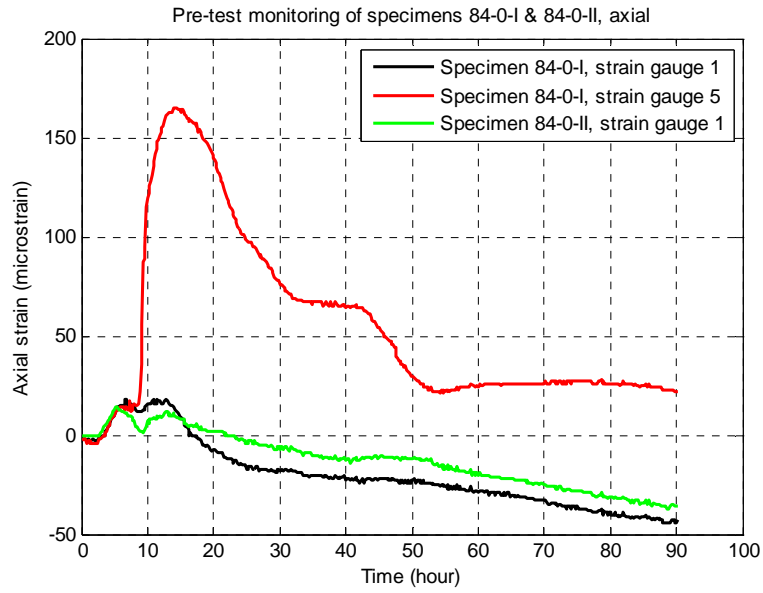


Figure 4.7 Failure mode of ring specimens under axial compression

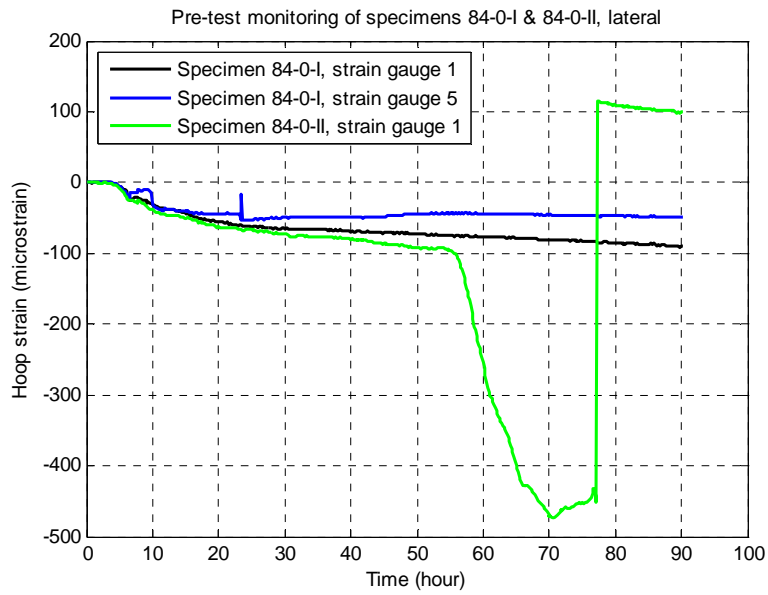


The arrangement of the strain gauge groups (left) and the strain gauge directions of each strain gauge group (right)

Figure 4.8 Layout of eight groups of strain gauges

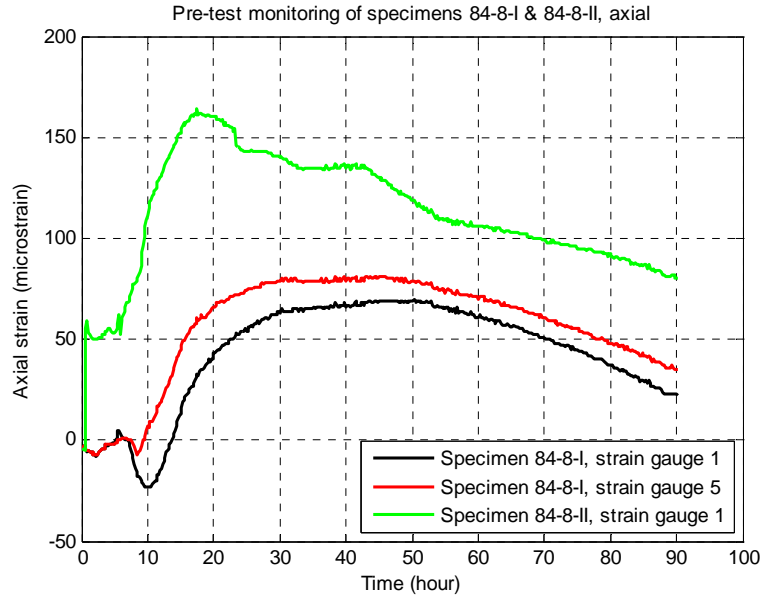


(a)

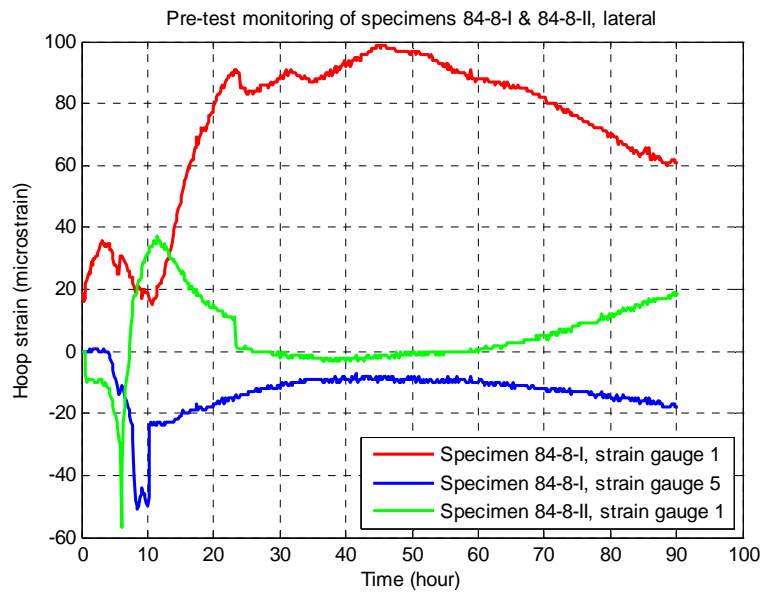


(b)

Figure 4.9 Pre-test monitoring results of specimens 84-0-I & 84-0-II

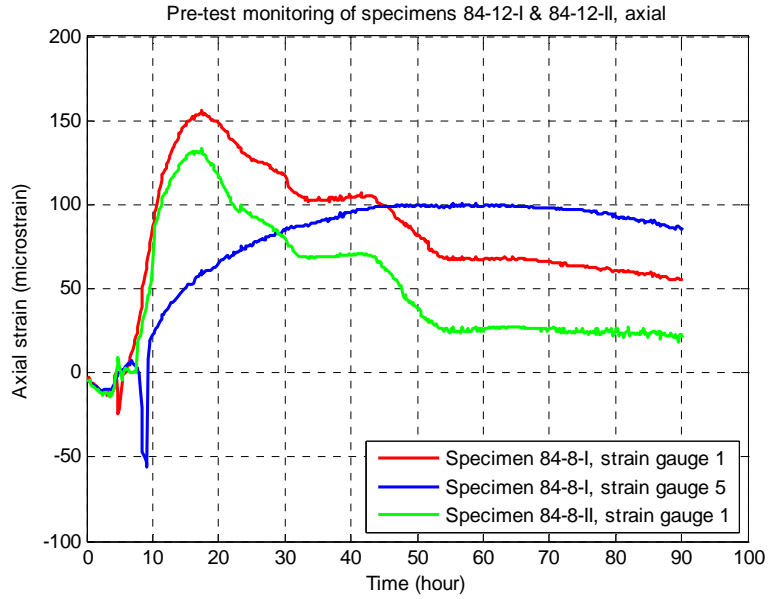


(a)

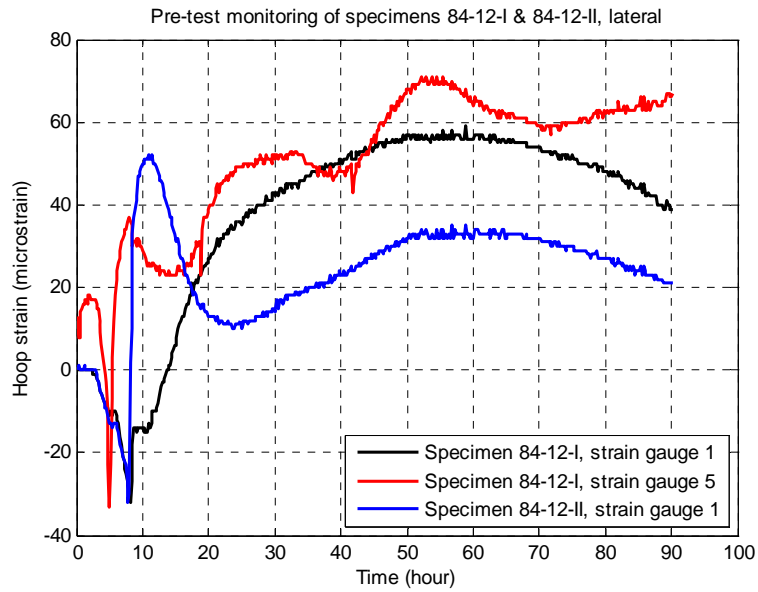


(b)

Figure 4.10 Pre-test monitoring results of specimens 84-8-I & 84-8-II



(a)



(b)

Figure 4.11 Pre-test monitoring results of specimens 84-12-I & 84-12-II



Figure 4.12 Pre-test monitoring and concrete curing



Figure 4.13 Failure mode of specimens 84-0-I & 84-0-II

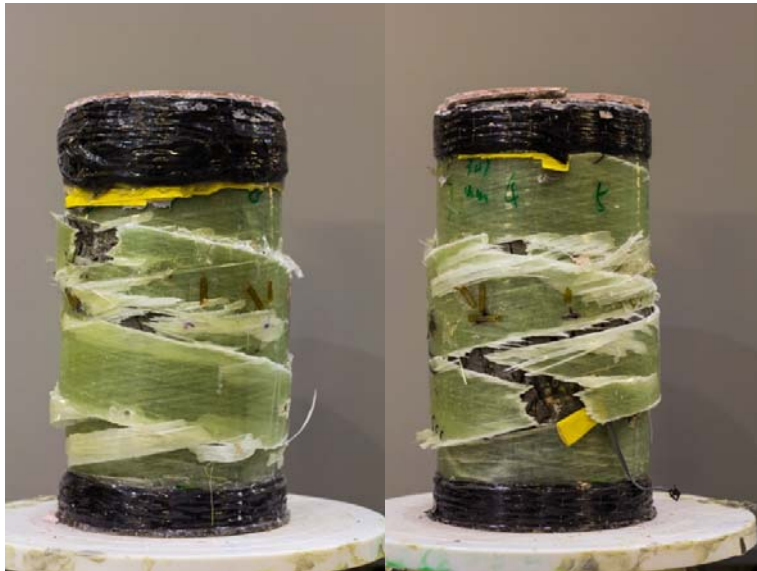
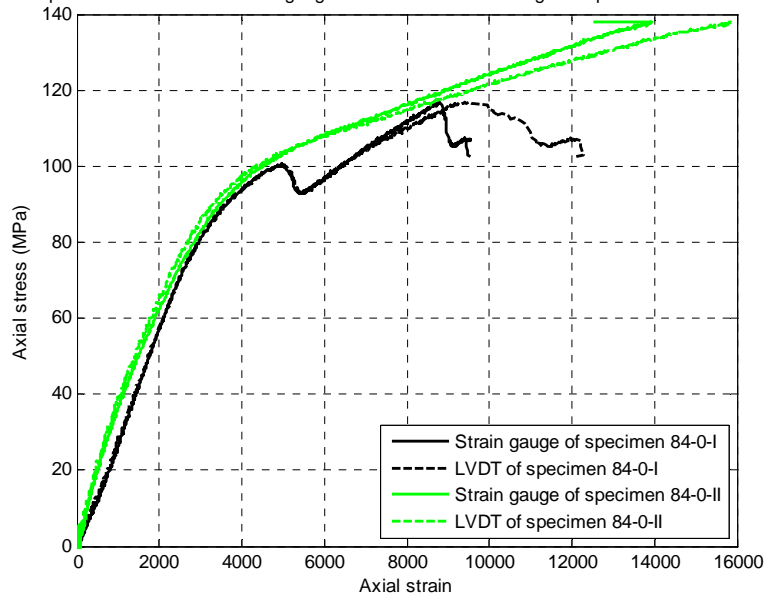


Figure 4.14 Failure mode of specimens 84-8-I & 84-8-II



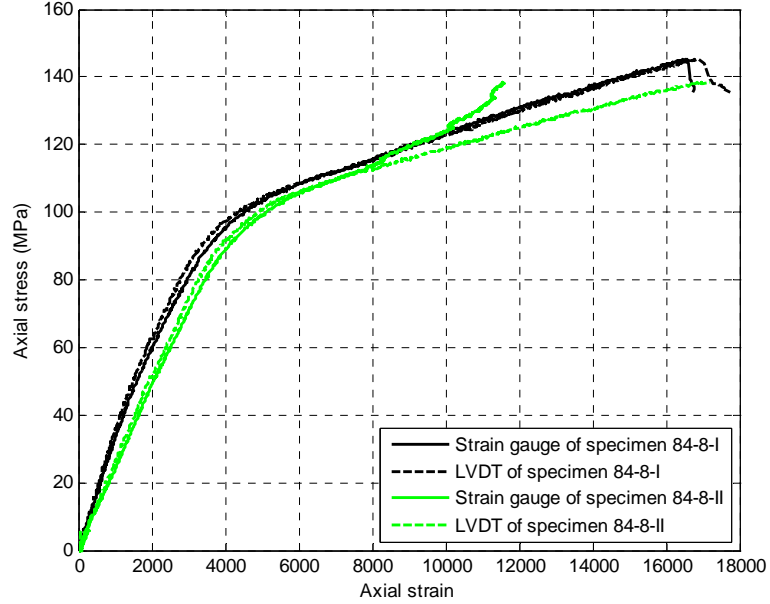
Figure 4.15 Failure mode of specimens 84-12-I & 84-12-II

Comparison between axial strain gauge values and LVDT readings for specimens 84-0-I & 84-0-II



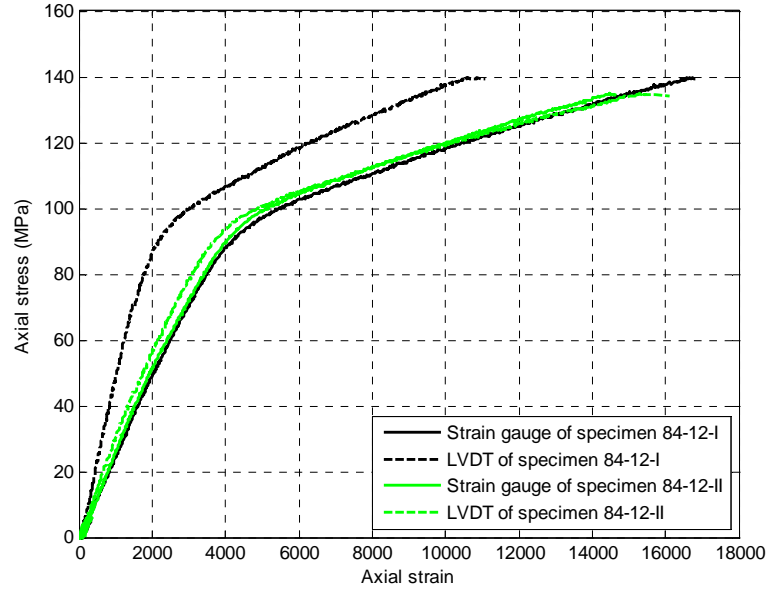
(a)

Comparison between axial strain gauge values and LVDT readings for specimens 84-8-I & 84-8-II



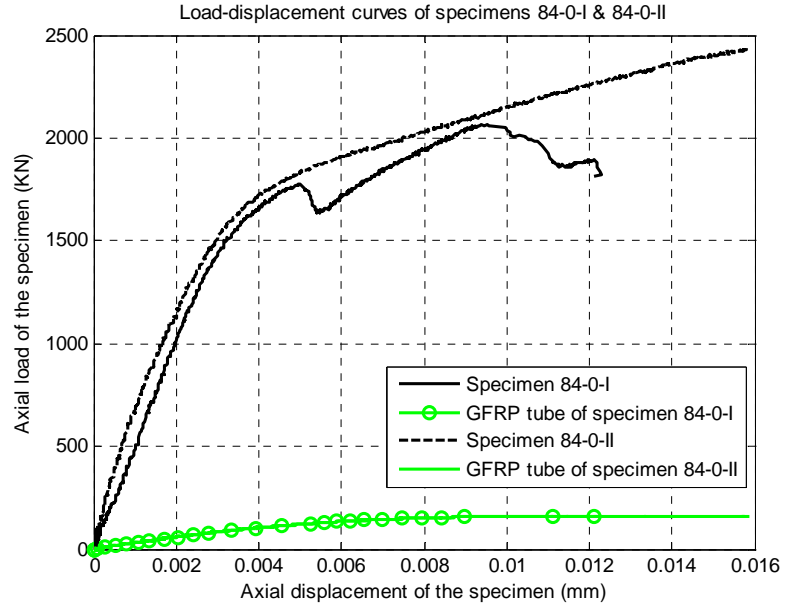
(b)

Comparison between axial strain gauge values and LVDT readings for specimens 84-12-I & 84-12-II

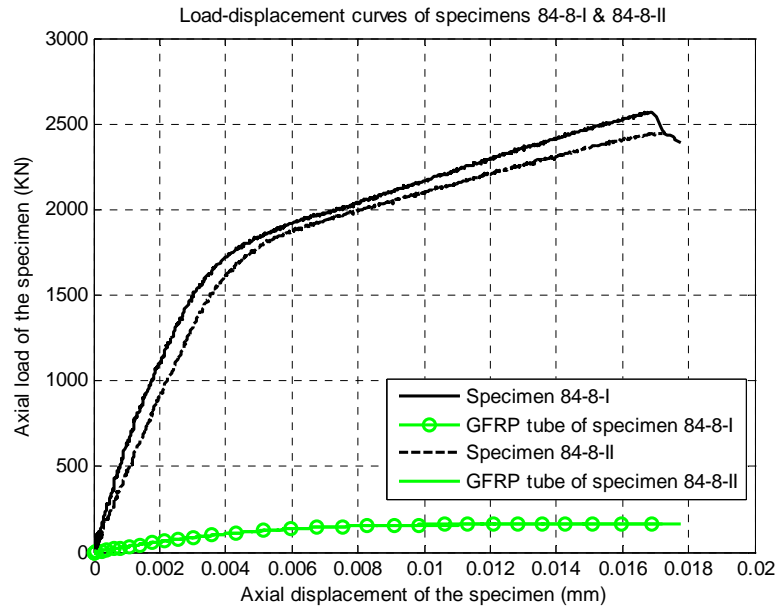


(c)

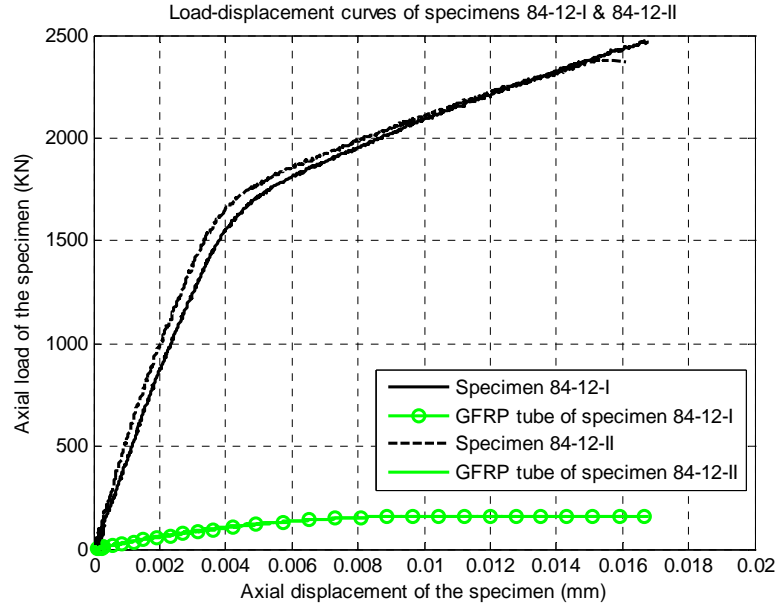
Figure 4.16 Comparison between axial strain gauge values and LVDT readings



(a)

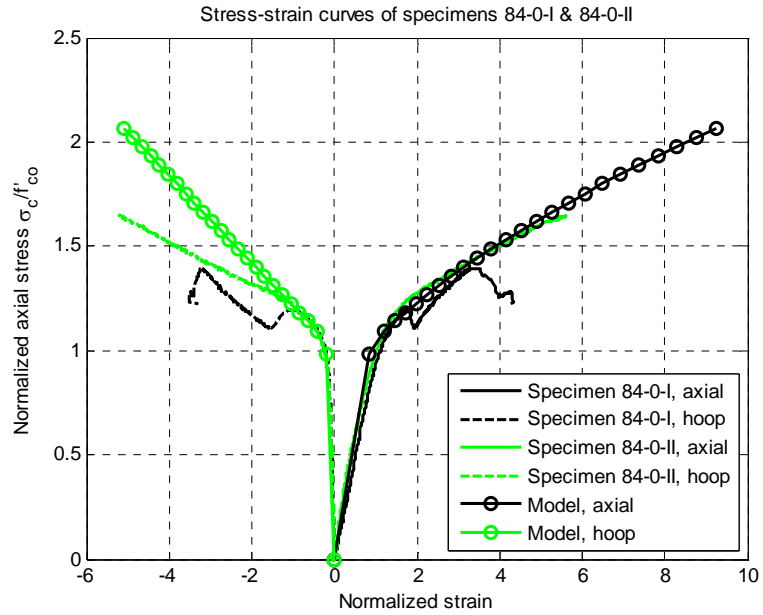


(b)



(c)

Figure 4.17 Load-displacement curves of specimens



(a)

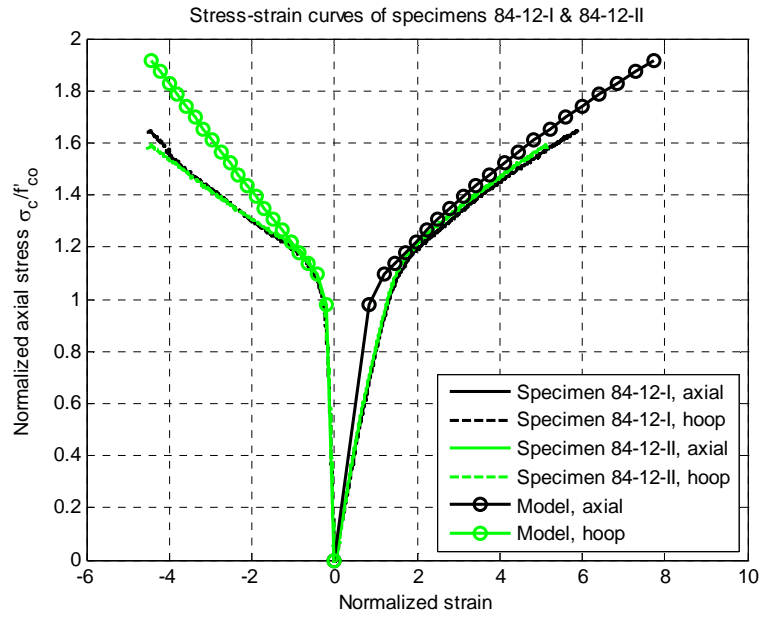
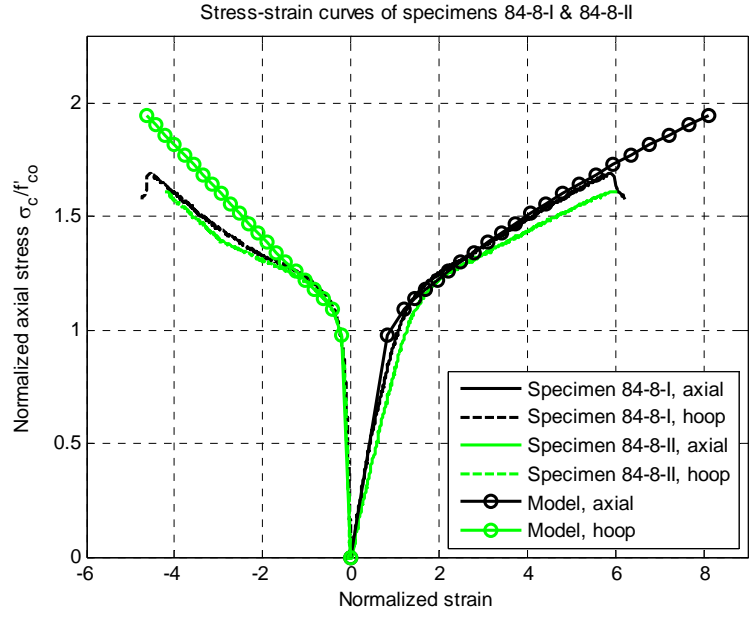
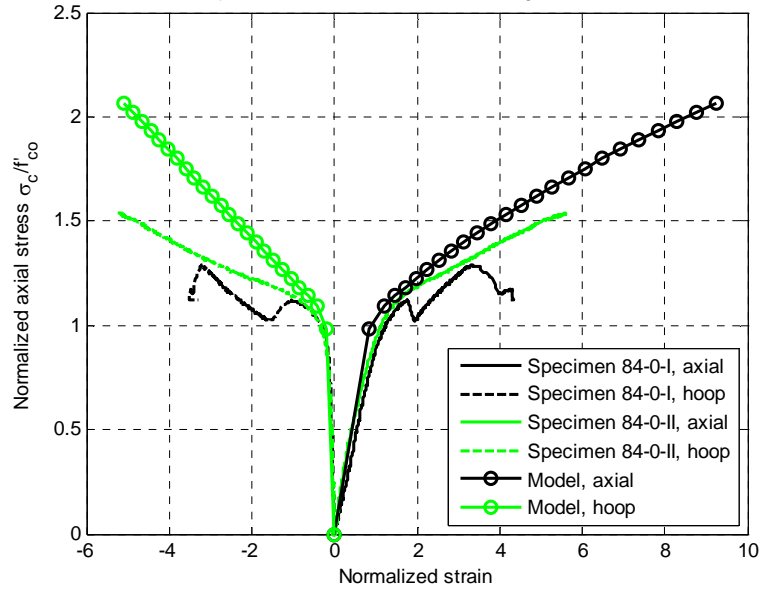


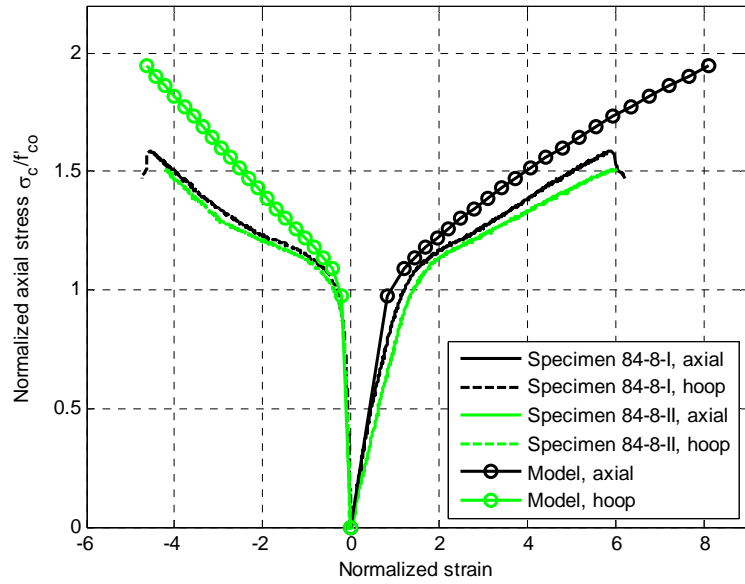
Figure 4.18 Stress-strain curves of SCC-filled GFRP tubes

Stress-strain curves of specimens 84-0-I & 84-0-II, excluding the GFRP tube axial contribution



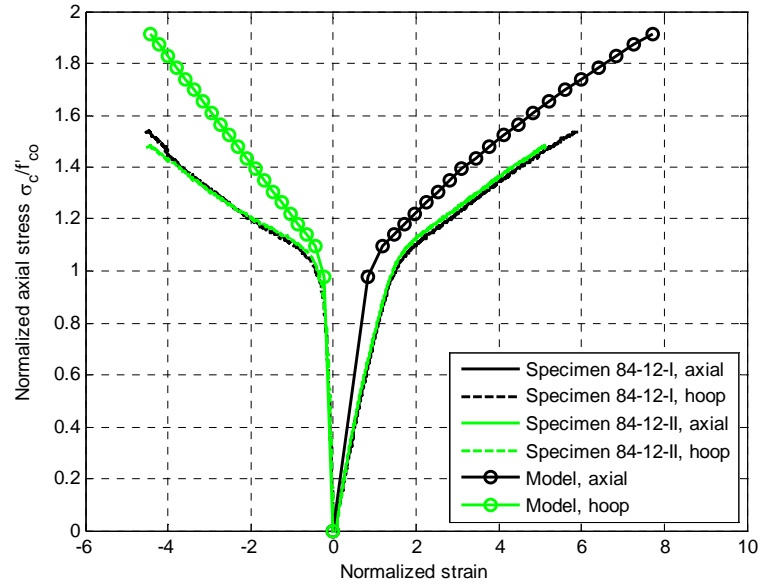
(a)

Stress-strain curves of specimens 84-8-I & 84-8-II, excluding the GFRP tube axial contribution



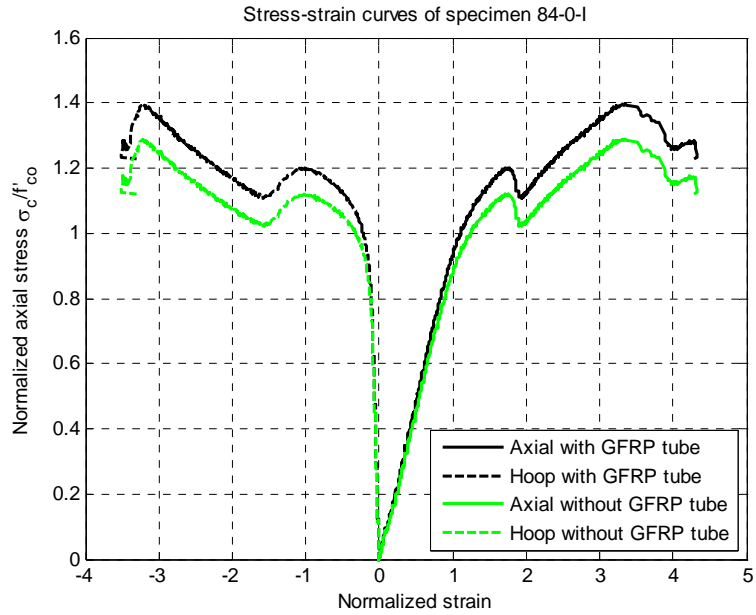
(b)

Stress-strain curves of specimens 84-12-I & 84-12-II, excluding the GFRP tube axial contribution

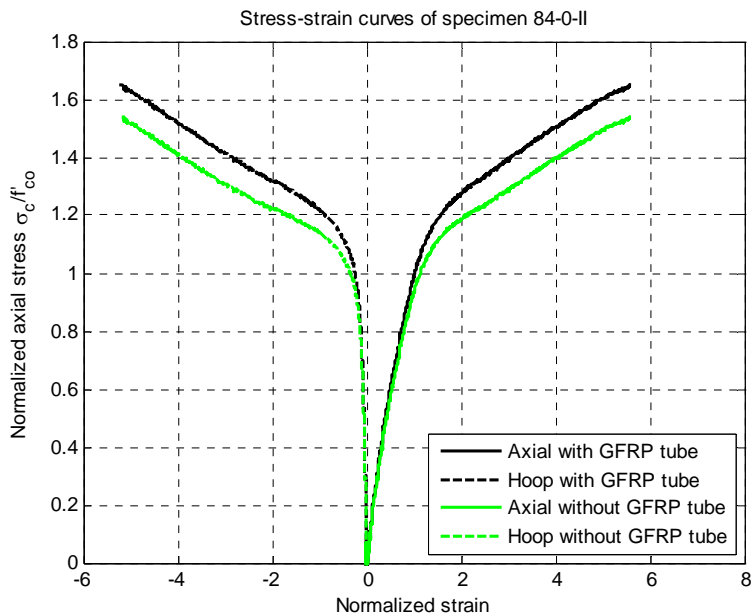


(c)

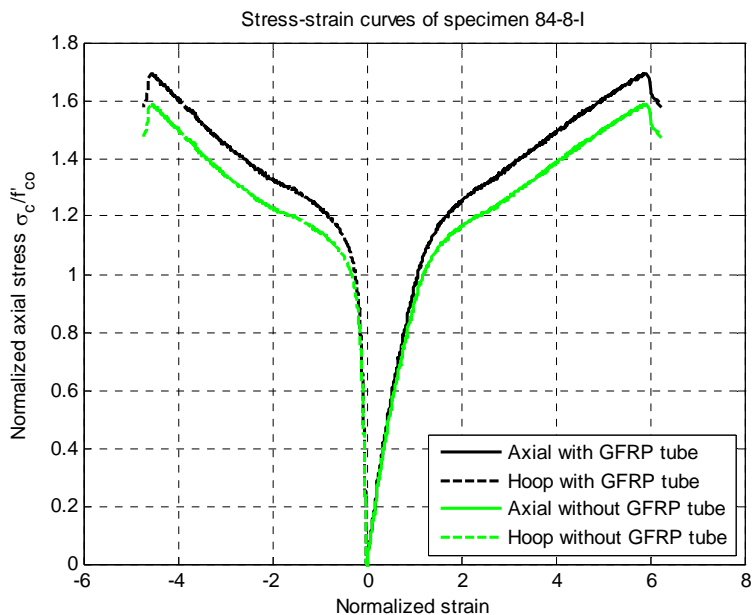
Figure 4.19 Stress-strain curves excluding the GFRP tube axial contribution



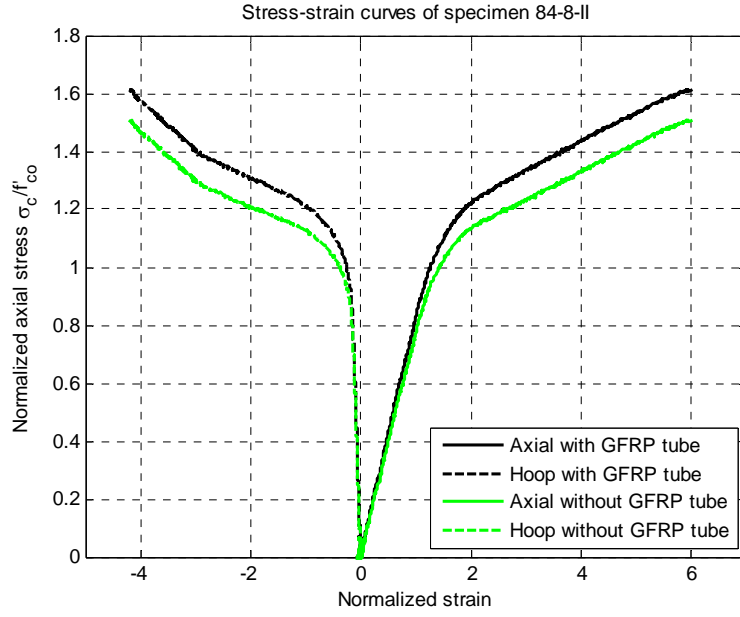
(a)



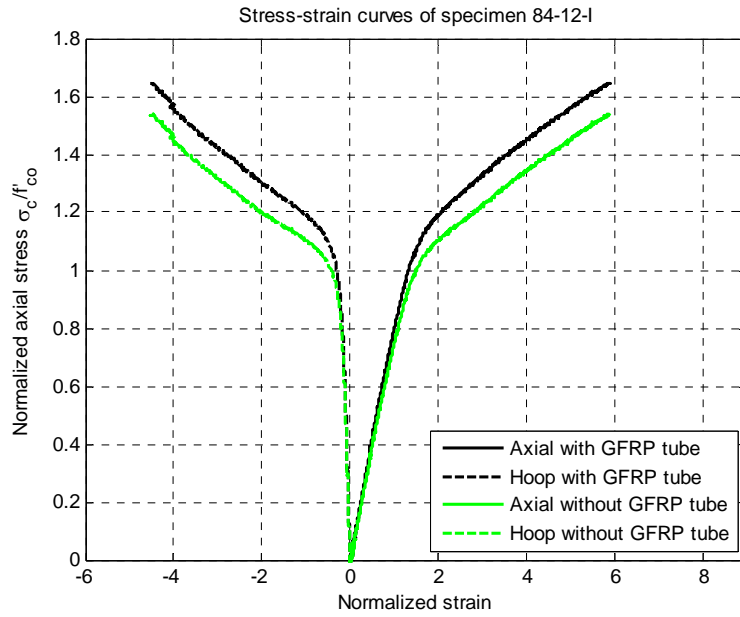
(b)



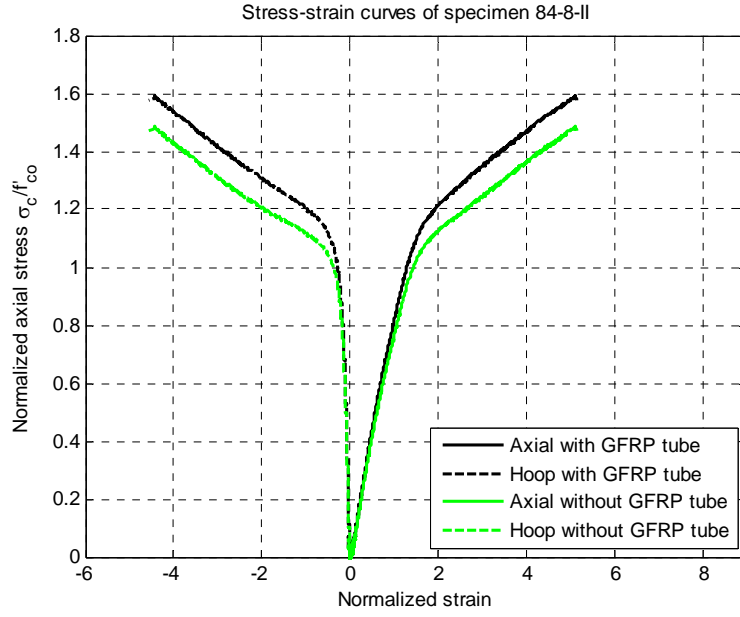
(c)



(d)

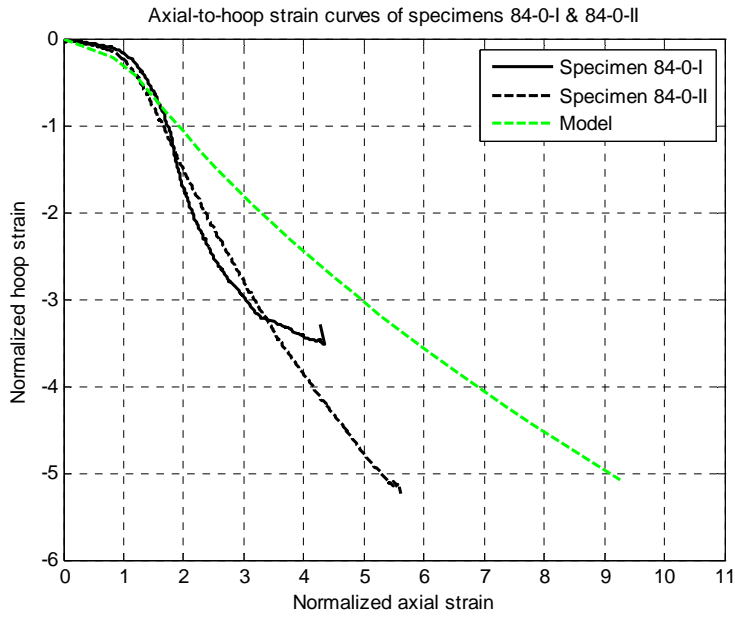


(d)

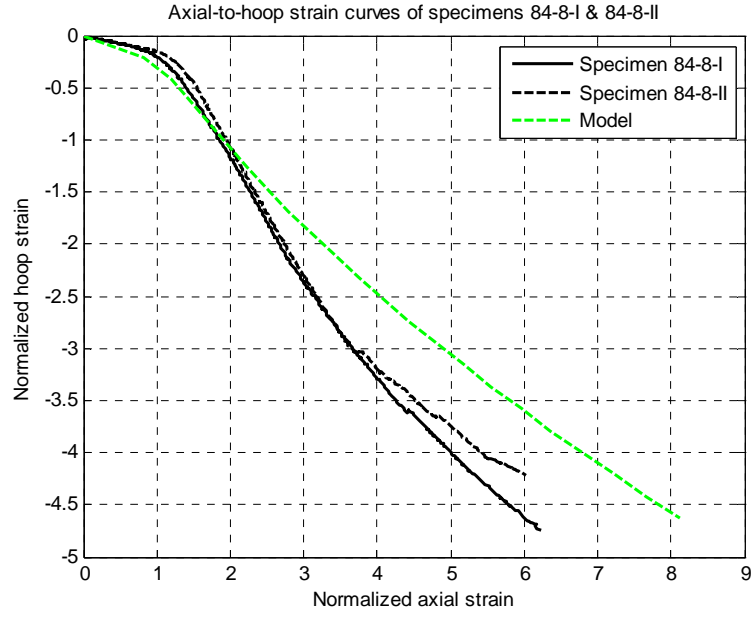


(e)

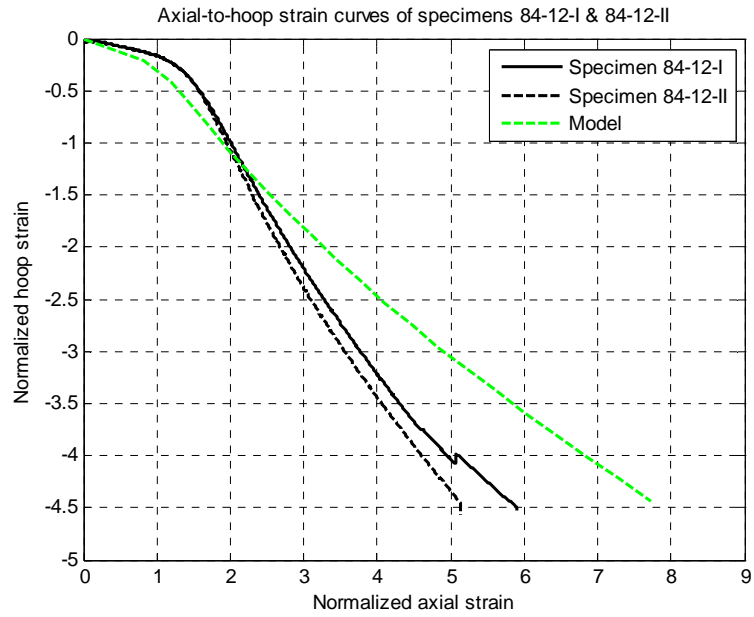
Figure 4.20 Stress-strain curves with and without GFRP tube axial contribution of the 6 specimens



(a)

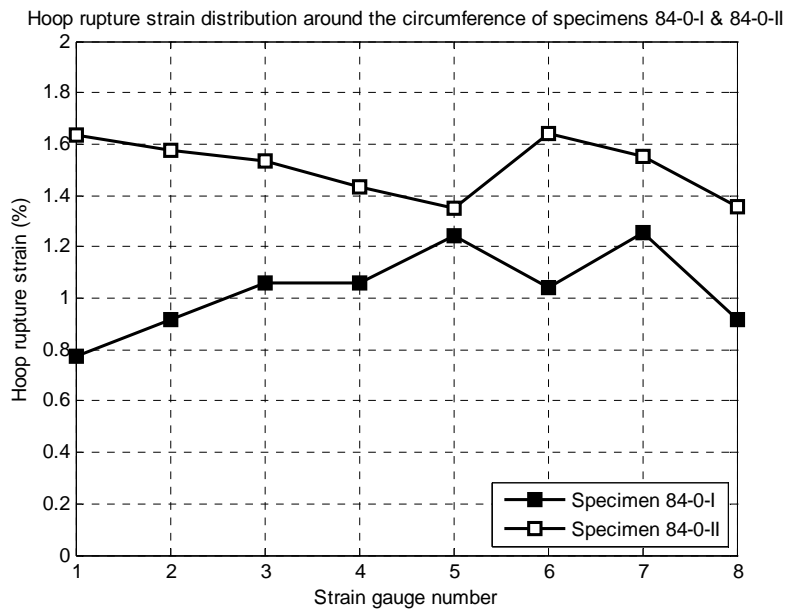


(b)

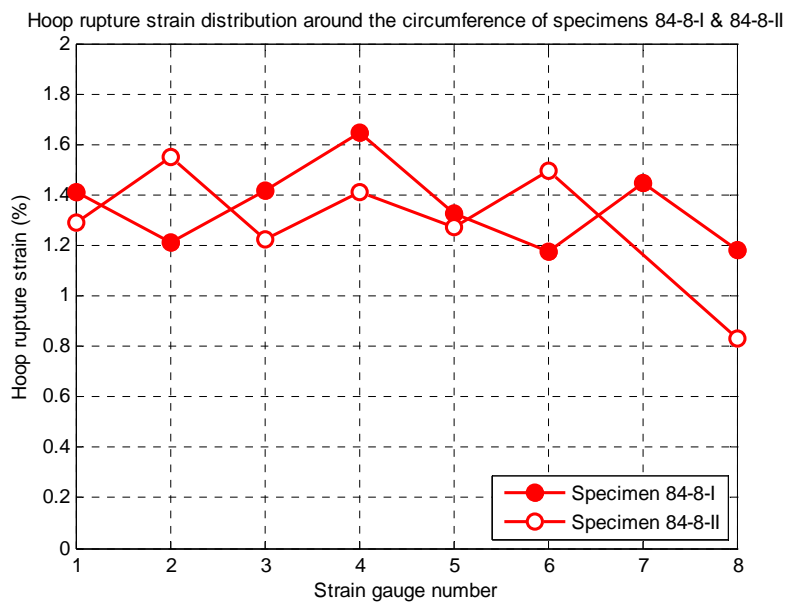


(c)

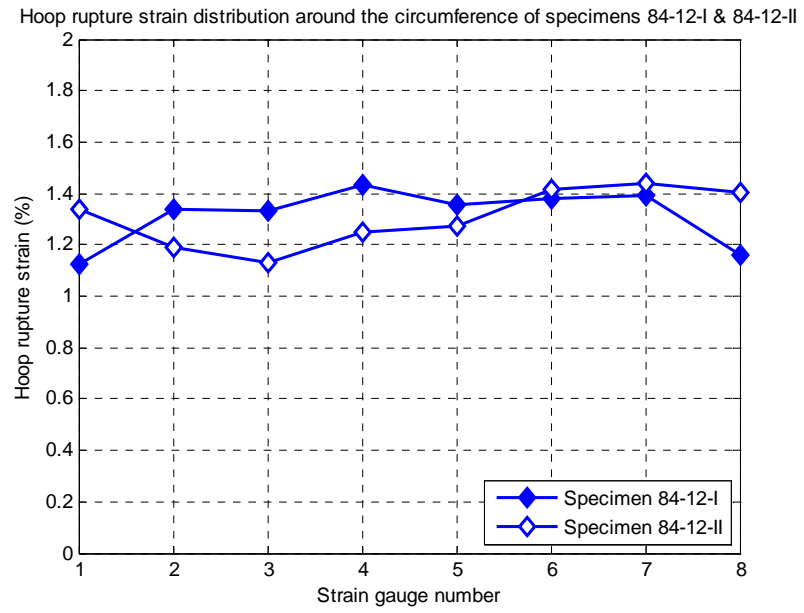
Figure 4.21 Axial-to-hoop strain curves of SCC-filled GFRP tubes



(a)



(b)



(c)

Figure 4.22 Hoop rupture strain distribution around the circumference of specimens

4.7 REFERENCES

- DETWILER, R. J. & MEHTA, P. K. 1989. Chemical and physical effects of silica fume on the mechanical behavior of concrete. *ACI Materials Journal*, Vol. 86, No. 6, pp. 609-614.
- DOMONE, P. 2007. A review of the hardened mechanical properties of self-compacting concrete. *Cement and Concrete Composites*, Vol. 29, No. 1, pp. 1-12.
- GB J119. 1988. *The Technical Standard for Concrete Admixture Application*. National Construction Standard of People's Republic of China (GB), Beijing, China
- GIBSON, R. F. 2012. *Principles of Composite Material Mechanics*, CRC press.
- JIANG, T. & TENG, J. G. 2007. Analysis-oriented stress–strain models for FRP–confined concrete. *Engineering Structures*, Vol. 29, No. 11, pp. 2968-2986.
- NAGATAKI, S. & GOMI, H. 1998. Expansive admixtures (mainly ettringite). *Cement and Concrete Composites*, Vol. 20, No. 2-3, pp. 163-170.
- TENG, J. G, HUANG, Y. L, LAM, L. & YE, L. 2007. Theoretical model for fiber-reinforced polymer-confined concrete. *Journal of Composites for Construction*, Vol. 11, No. 2, pp. 201-210.
- Zhang, B. 2014. *Hybrid FRP-Concrete-Steel Double-Skin Tubular Columns under Static and Cyclic Loading*, PhD thesis, The Hong Kong Polytechnic University, Hong Kong, China, in preparation.

CHAPTER 5

CONCLUSIONS

5.1 INTRODUCTION

It is attractive to use self-compacting concrete (SCC) to fill GFRP tubes to construct high-performance columns. The GFRP tube serves as the stay-in-place form and provides external confinement to the concrete core. This thesis has therefore presented a study into the behavior of SCC as confined in GFRP tubes. The study has paid particular attention to the similarities and differences between SCC and normal concrete (NC) under axial compression and with FRP confinement.

The experimental program of the study was focused on the compressive behavior of SCC with confinement from an FRP wrap or a filament-wound GFRP tube. Results from associated material tests were also presented in the thesis. These tests were mainly to reveal the behavior of confined SCC. The test results were compared with predictions of an analytical model for FRP-confined NC.

5.2 COMPRESSIVE BEHAVIOR OF SCC CONFINED BY FRP WRAPS

A series of axial compression tests on SCC confined with FRP wraps with fibres oriented

in the hoop direction was conducted. The test results showed that the behavior of such FRP-confined SCC is generally similar to that of FRP-confined normal concrete (NC); the unconfined concrete strength, the stiffness of the FRP wrap, and the hoop strain capacity of the FRP jacket all have a similar effect on behavior for these two types of confined concrete. (Jiang and Teng, 2007) model, which was originally developed for FRP-confined NC, has been shown to provide reasonably close predictions for FRP-confined SCC, especially for the axial stress-strain curves of moderately confined normal strength SCC and heavily confined high strength SCC. Although the behavior of SCC under weak FRP confinement is not well predicted by (Jiang and Teng, 2007) model, this is not a significant issue as such weak confinement is unlikely to arise in hybrid FRP-concrete tubular columns. The experimental results indicated that: (1) at the same axial strain, the lateral expansion of FRP-confined SCC is larger, leading to a larger confining pressure; (2) at the same axial strain and the same confining pressure, the axial stress of FRP-confined SCC is smaller. The combination of the two effects means that the axial stress-strain curves of FRP-confined SCC can be closely approximated by a stress-strain model developed for FRP-confined NC, but the relationship between the ultimate axial strain and the ultimate hoop rupture strain may need to be improved. This is an important conclusion as it means that design rules developed for hybrid FRP-concrete tubular columns cast with NC can be assumed to be directly applicable to such members cast with SCC, and vice versa. In addition, it should be noted that the use of mineral admixtures (e.g. silica fume and GBFS) may influence the behavior of FRP-confined concrete, and some research is needed to ascertain the effect when or where such use makes this

influence a significant issue.

5.3 COMPRESSIVE BEHAVIOR OF SCC CONFINED BY GFRP TUBES

A series of compression test on SCC-filled GFRP tubes was conducted to understand the behavior of SCC as confined by GFRP tubes. These GFRP tubes had fibers oriented at ± 80 degrees to the longitudinal axis, so their major stiffness/strength direction is the hoop-direction. Their material properties were evaluated with the help of appropriate material tests as well as the lamination theory.

An expansive admixture was included in the concrete mix design for some of the test specimens to compensate for the expected shrinkage of SCC or even to create some pre-tension in the hoop direction of the GFRP tube. The test results showed that by using a suitable amount of expansive admixture, the confinement condition of SCC in GFRP tubes was significantly improved without causing significant changes in the SCC properties. It is recommended that in practice, a suitable amount of expansive admixture should be included when SCC is used to construct SCC-filled FRP tubular columns to eliminate the detrimental effect of a shrinkage-induced gap between the SCC and the FRP tube.

(Jiang and Teng, 2007) analysis-oriented stress-strain model, which was developed for normal concrete confined by unidirectional FRP wraps with fibers in the hoop direction,

was adopted as the theoretical reference to make predictions. The results from (Jiang and Teng, 2007) model was found to be in reasonably close agreement with the test results for SCC confined by FRP tubes if only the axial stress-strain behavior is considered. However, the axial-hoop strain response of SCC confined by GFRP tubes differs significantly from that predicted by (Jiang and Teng, 2007) model, and this observation is consistent with the conclusion for SCC confined by FRP wraps with fibers in the hoop direction.

5.4 FUTURE RESEARCH

Comparisons between predictions from (Jiang and Teng, 2007) for FRP-confined NC and the tests results of SCC confined by either FRP wraps or GFRP tubes have shown that although the two types of concrete have similar axial stress-axial strain responses, they differ in the lateral expansion behavior. The lack of accuracy of (Jiang and Teng, 2007) model in predicting the lateral behavior of confined SCC means that the ultimate state of FRP-confined SCC cannot be accurately predicted even if the ultimate hoop strain of the FRP wrap/tube is known. Therefore, research needs to be conducted in the future to develop a stress-strain model that can capture both the axial and lateral responses of FRP-confined SCC.

The effect of the greater shrinkage experienced by SCC on the behavior of SCC confined by FRP tubes and its compensation using an expansive admixture was studied in the present thesis using small diameter GFRP tubes. This phenomenon may be size-related,

and should be further studied using larger-diameter GFRP tubes. Further experimental work to clarify the reason for the sudden drop in the axial stress also needs to be conducted.